This manuscript was published by Superconductor Science & Technology (SuST, IOP) 27, No. 4, 044001, (2014).

Challenges and Status of ITER Conductor Production

A. Devred, I. Backbier, D. Bessette, G. Bevillard, M. Gardner, C. Jong, F. Lillaz, N. Mitchell, G. Romano and A. Vostner

Magnet Division, ITER International Organization, Route de Vinon-sur-Verdon, 13115 St Paul-Les-Durance, France

Abstract

Taking the relay of the Large Hadron Collider (LHC) at CERN, ITER has become the largest project in applied superconductivity. In addition to its technical complexity, ITER is also a management challenge as it relies on an unprecedented collaboration of 7 partners, representing more than half of the world population, who provide 90% of the components as in-kind contributions. The ITER magnet system has a stored energy of 51 GJ and involves 6 of the ITER partners. The coils are wound from Cable-In-Conduit Conductors (CICCs) made up of superconducting and copper strands assembled into a fully transposed, rope-type cable, inserted into a conduit of butt-welded austenitic steel tubes. The conductors for the Toroidal Field (TF) and Central Solenoid (CS) coils require about 500 tons of Nb_3Sn strands while the Poloidal Field (PF) and Correction Coil (CC) and busbar conductors need around 250 tons of Nb–Ti strands. The required amount of Nb_3Sn strands far exceeds pre-existing industrial capacity and has called for a significant worldwide production scale up. The TF conductors are the first ITER components to be mass produced and are more than 50% complete. During its life time, the CS coil will have to sustain several tens of thousands of electromagnetic (EM) cycles to high current and field conditions, way beyond anything a large Nb_3Sn coil has ever experienced. Following a comprehensive R&D program, a technical solution has been found for the CS conductor, which ensures stable performance versus EM and thermal cycling. Productions of PF, CC and busbar conductors are also underway. After an introduction to the ITER project and magnet system, we describe the ITER conductor procurements and the Quality Assurance/Quality Control programs that have been implemented to ensure production uniformity across numerous suppliers. Then, we provide examples of technical challenges that have been encountered and we present a status of ITER conductor production worldwide.

1. ITER Project

The main goal of the ITER project is to demonstrate the scientific and technological feasibility of fusion power [1,2]. This includes in particular: 1) the achievement of extended burn of Deuterium-Tritium plasmas, with steady state as the ultimate goal, 2) the integration and test of all critical fusion power reactor technologies and components, including the sophisticated magnet system at the heart of the machine, and 3) the demonstration of the safety and environmental acceptability of nuclear fusion.

This manuscript was submitted to Superconductor Science & Technology (IOP) for possible publication
This manuscript was published by Superconductor Science & Technology (SuST, IOP) 27, No. 4, 044001, (2014).

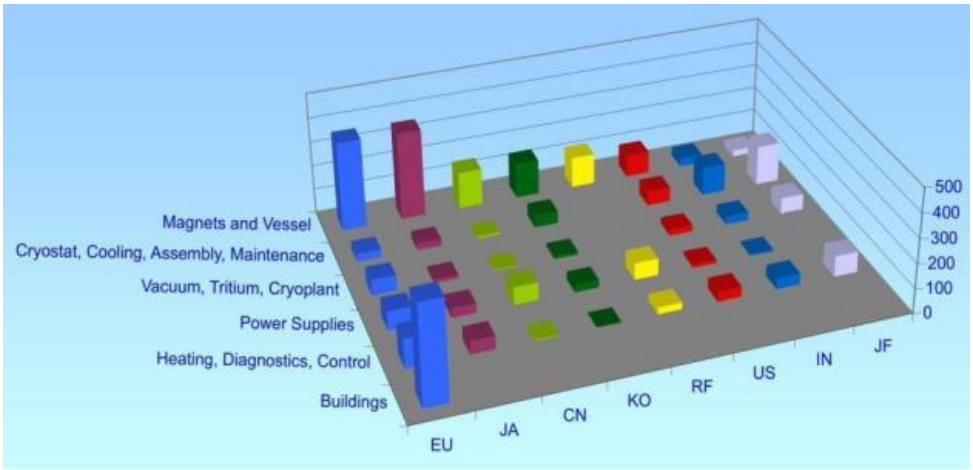

Figure 1: Procurement allocation among ITER partners: EU (Europe), JA (Japan), CN (China), KO (Korea), US (United States), IN (India) and JF (Joint Funds).

ITER is also an unprecedented political and management challenge. It was born in 1985 at a superpower summit meeting in Geneva between R. Reagan and M. Gorbachev. It is now supported by 7 members: China (CN), Europe (EU), India (IN), Korea (KO), Japan (JA), the Russian Federation (RF) and the United States (US), representing more than half of the world's population. The 7 ITER members have agreed a procurement allocation, based on an overall agreed procurement value for the project's construction phase, of which EU assumes responsibility for 5/11th of the overall value while each of the other members will support the project with a share of 1/11th. The bulk of the contributions, in terms of technologies and industrial productions, is to be delivered in kind - about 90% of the overall value, while the remaining 10% will be in cash contributions, also referred to as joint funds (JF). The breakdown of who contributes what is at the component level and is cast in the *so-called* ITER Agreement. Figure 1 illustrates this task sharing. All members except India contribute to the magnet system.

The project is managed by the International Organization (IO) and the 7 members have set up Domestic Agencies (DAs) to handle their contributions. The IO is responsible for overall design and integration, defines the technical requirements and issues Procurement Arrangements (PAs) with the DAs. The DAs carry out calls for tender (following domestic rules), procure the components and deliver them to the IO within the PA framework.

The ITER site was selected in 2005 near Saint-Paul-Les-Durance in the South of France. As part of a special contribution to the project, France has completed massive roadwork for transportation of large components from Marseille harbor about 104 km away. Civil engineering has been underway on the ITER platform since 2010 and the French Government authorized the nuclear installation creation in November 2012. As illustrated in Figure 2, which shows recent pictures of the ITER site, two buildings have been completed: the large (252 m x 45 m x 17 m) building to be used for the on-site manufacturing of the Poloidal Field (PF) coils and the headquarter building. The excavation of the tokamak pit (120 m x 90 m x 17 m) and the foundation of the tokamak building, which include 493 x 1.8 m high seismic pads covered by a 1.5-meter-thick basemat, have also been completed.

This manuscript was submitted to Superconductor Science & Technology (IOP) for possible publication
This manuscript was published by Superconductor Science & Technology (SuST, IOP) 27, No. 4, 044001, (2014).

Figure 2: Recent views from ITER construction site, near Saint-Paul-Les-Durance, France.

2. ITER Tokamak and Magnet System

ITER relies on the tokamak concept first proposed by I. Y. Tamm and A. Sakharov in the 1950's. The main components of the ITER tokamak are [3]

- the vacuum vessel (which delimits the plasma chamber),
- the magnet system (which controls plasma confinement, shaping and stability),
- the cryostat (which shields the vacuum vessel and the magnet system),
- the blankets and divertor (which absorb neutron flux and eliminate plasma ashes).

As illustrated in Figure 3, the tokamak cryostat is 28 m tall and 29 m in diameter, which corresponds more or less to the size of the Jefferson memorial in Washington DC.

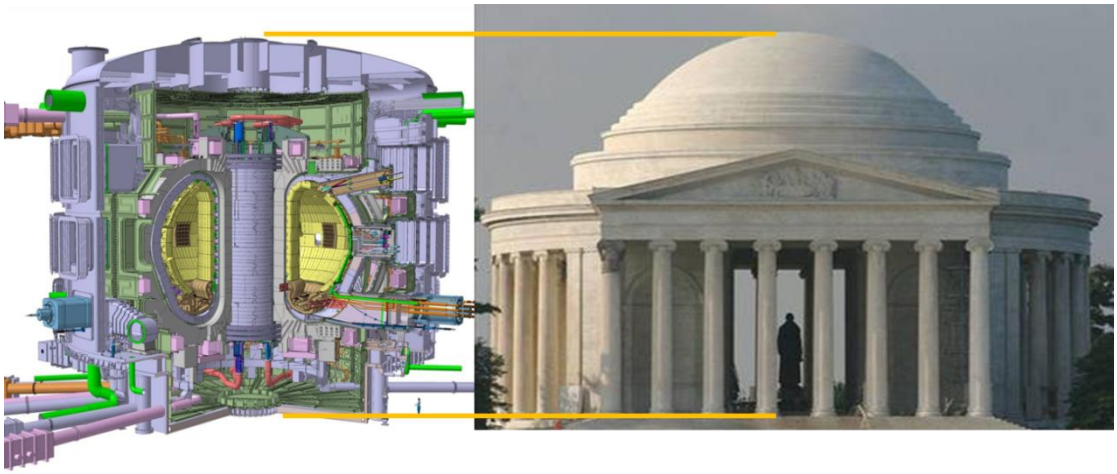

Figure 3: Artist view of the ITER tokamak (~28 m tall x 29 m in diameter) in comparison the Jefferson Memorial in Washington DC (29 m tall; courtesy of G. Johnson).

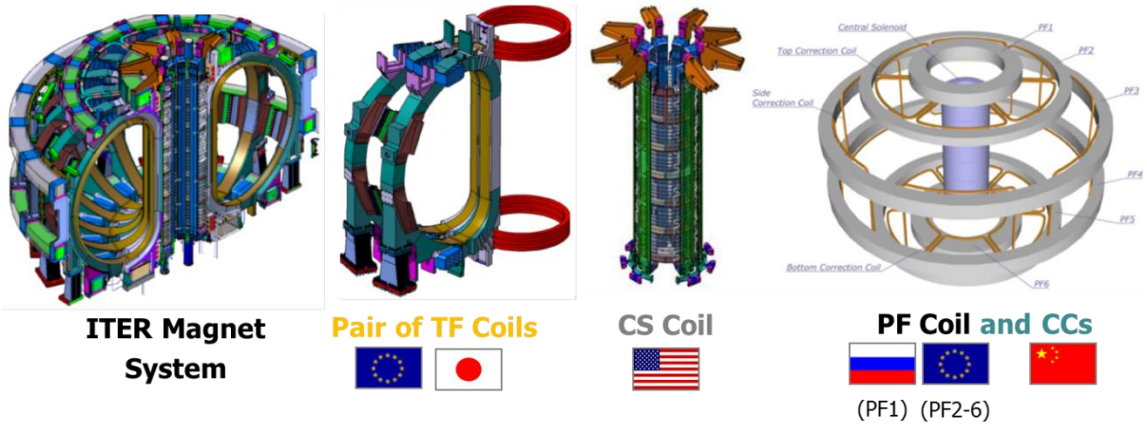

Figure 4: Artist views of the ITER magnet system and of the different coils that make it up: TF (toroidal field), CS (central solenoid), PF (polidal field) and CC (correction coils).

The ITER magnet system is fully superconducting and includes 4 different types of coils (see Figure 4) [4]

- 18 Toroidal Field (TF) coils, located around the plasma chamber, to be manufactured in EU [5] and Japan [6],
- a Central Solenoid (CS), made up of a stack of 6 modules and positioned at the machine centre, to be manufactured in the US [7],
- 6 Poloidal Field (PF) coils, surrounding the TF coils, whose manufacture is the responsibility of RF (for PF1) and EU (for PF2 to 6) [8],
- 9 pairs of Correction Coils (CCs), attached to the PF coils, to be manufactured in China [9].

The ITER magnets are supplied with current and cryogenic fluids by means of 31 Feeders. The feeders count more than 600,000 parts and are deeply embedded inside the tokamak with many interfaces [10]. They include two types of superconducting busbars: the Main Busbars (MB), supplying the TF, CS and PF coils and the Correction coil Busbars (CB) supplying the CCs. They also include 60 High Temperature Superconductor (HTS) current leads of various types [11]. The HTS lead designs rely on BSCCO 2223/Ag-Au tapes, with fin-type heat exchanger extrapolated from the HTS lead designs developed by CERN for the Large Hadron Collider (LHC). The feeders, busbar conductors and HTS leads are built-to-print packages procured in kind by China.

The ITER magnet system is the largest and most integrated superconducting magnet system ever built. Its stored magnetic energy is 51 GJ. As a comparison, the second largest superconducting magnet system is the Large Hadron Collider machine at CERN, which has a stored magnetic energy of ~11 GJ distributed over a magnet ring of 27 km in circumference [12]. In case of a quench, the ITER magnet system is expected to be discharged in about 10 s. Of course, this raises tremendous challenges for magnet protection and for the quench detection systems which have to be operated in a very noisy electromagnetic environment, with enough sensitivity to discriminate between resistive voltage increases in the coils and false triggers due to plasma disruptions [13].

Figure 5. Views of the ITER TF conductors and of its components (courtesy of P. Lee and C. Sanabria, Florida State University).

3. ITER Conductors

ITER magnets rely on Cable-In-Conduit Conductors (CICCs), a concept developed in the mid 1970's by M.O. Hoenig [14]. As illustrated in Figure 5, the main features of the ITER CICCs are [15]

- Cr-plated Nb_3Sn or Ni-plated Nb–Ti superconducting (sc) strands mixed with segregated Cr-plated or Ni-plated Cu strands,
- a multi-stage cable with stainless steel cable/sub-cable wraps and a central cooling spiral (save for CC and MB conductors),
- a circular, square or circle-in-square, austenitic stainless steel conduit made up of butt-welded jacket sections.

The TF and CS conductors both rely on Cr-plated Nb_3Sn strands, while the PF, CC, MB and CB conductors rely on Ni-plated Nb–Ti strands [15]. The TF, MB and CB conductors have a circular jacket, the CS and PF conductors have a circle-in-square jacket, while the CC conductor is square. TF conductors are manufactured by 6 DAs: CN [16-17], EU [18], JA[19], KO[20], RF [21] and US. CS conductors are the responsibility of JA but are funded by the EU as part of the Broader Approach agreement negotiated between Japan and Europe at the time of site selection [22]. Conductors for PF1 and PF6 coils are manufactured by RF and EU, which have signed a bilateral agreement upon which RF takes care of strand production and cabling and EU takes care of the rest of conductor production [18;21]. CC [23], MB and CB [24] conductors are the responsibility of CN. A typical TF Conductor Unit Length is ~760 m and requires a minimum of 3.3 t of Nb_3Sn strands and 1.6 t of stainless steel tubes. A typical CS Conductor Unit Length is ~900 m and requires a minimum of 2.6 t of Nb_3Sn strands and 11.3 t of stainless steel tubes. In the case of TF, the cost of the jacket is less than 10% of the cost of the strands, but for CS, it may be 50% or more. Let us note that the TF conductor package is one among a few that involves so many DAs.

This manuscript was submitted to Superconductor Science & Technology (IOP) for possible publication
This manuscript was published by Superconductor Science & Technology (SuST, IOP) 27, No. 4, 044001, (2014).

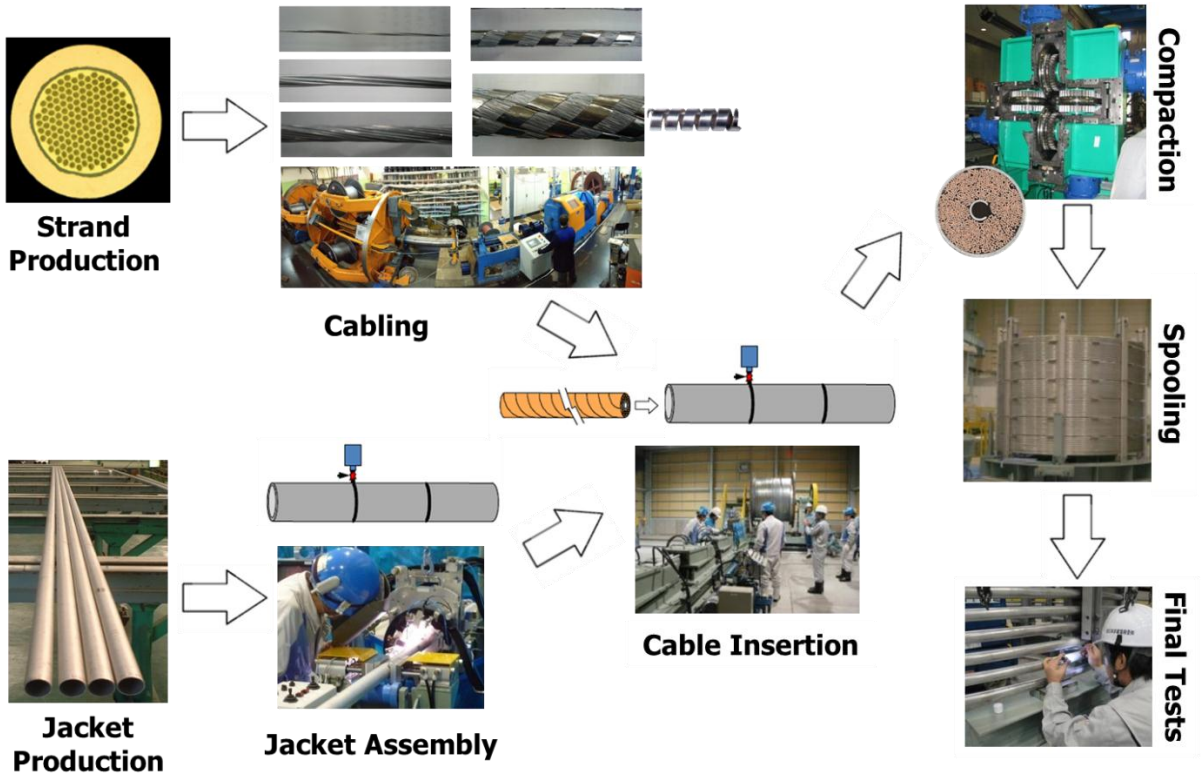

Figure 6: Main steps of ITER CICC manufacture (photos courtesy of D. Kaverin, VNIIKP and Y. Nunoya, JAEA).

Figure 6 details the main steps of conductor manufacture. It starts with strand production, relying on conventional extrusion and drawing techniques. The rope-type cables are manufactured in 5 stages (save for CC which has only 4) on dedicated machines designed to apply full back twist. The first cable stage is a triplet, usually made up of two superconducting strands and one copper strand, while the last stage is cabled on a planetary machine. The base material for the jacket is high purity austenitic steel and the jacket sections are produced by hot extrusion followed by cold drawing and/or pilgering steps and are carefully inspected by non-destructive examination (NDE) techniques. The jacket sections are butt-welded together to form a jacket assembly with a length corresponding to the final length of the conductor (up to 760 m for the TF conductors and 920 m for the CS conductors). Each orbital weld is inspected by X-rays and is subjected to a local helium leak check and a dye penetrant test. The inner diameter of the jacket assembly is a few millimetres larger than the cable outer diameter to enable its insertion by means of a pulling rope. Once the cable is inserted, the jacket is compacted to achieve final dimension and the compacted conductor is spooled over a diameter of ~4 m to facilitate transportation. The spooled conductor is subjected to a number of final acceptance tests, including a global helium leak test and another set of dye penetrant tests of every butt-weld.

This manuscript was submitted to Superconductor Science & Technology (IOP) for possible publication
This manuscript was published by Superconductor Science & Technology (SuST, IOP) 27, No. 4, 044001, (2014).

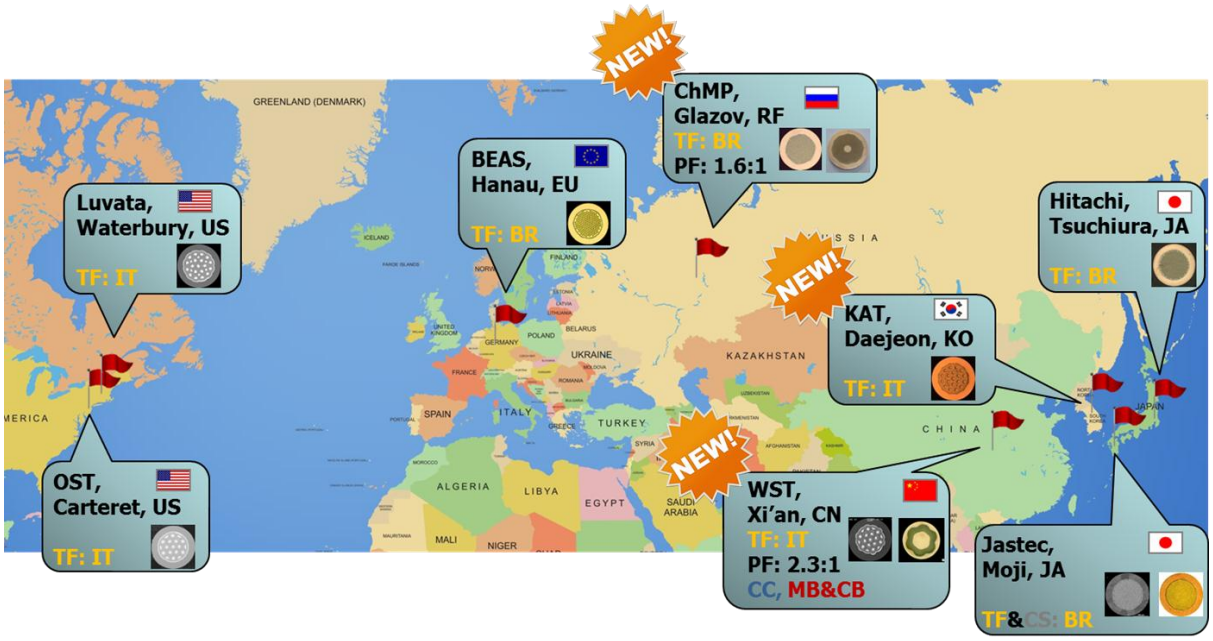

Figure 7: ITER strand suppliers around the world: a truly international collaboration. TF Nb_3Sn strands involve 4 bronze (BR) suppliers (BEAS, ChMP, Hitachi and Jastec) and 4 IT suppliers (KAT, Luvata, OST and WST). Nb–Ti strand type 1 is produced by ChMP, while Nb–Ti strand type 2 is produced by WST. So far, one bronze supplier has been selected for CS Nb_3Sn strands (Jastec).

For TF, which calls for an estimated amount of 480 tons of Nb_3Sn strands, 8 strand suppliers are involved: 4 rely on the bronze process and 4 rely on the Internal Tin (IT) process. For CS, so far, only one supplier of bronze process strands has been selected, this is because the procurement was only launched last year for the bottom module of the CS coil stack. Regarding Nb–Ti strands, 2 strand types are needed, one with a copper-to-non-copper ratio of 1.6 to 1 for the PF1&6 conductors (referred to as strand type 1) and one with a copper-to-non-copper ratio of 2.3 to 2 for all the other Nb–Ti conductors (PF2-5, CC, MB and CB; referred to as strand type 2). ChMP in RF has been selected for the production of strand type 1, while WST in China has been selected for the production of strand type 2. Figure 7 shows the distribution of strand suppliers, thereby confirming the international nature of the project. It should be noted that 3 of these suppliers (ChMP in RF [25], KAT in KO [26] and WST [27-28] in CN) are new to the business and have been set up by their government to fulfil the ITER needs, while the five others (BEAS in EU [29], Hitachi [30;32] and Jastec [31-32] in Japan and Luvata [33] and OST [34-35] in the USA) are well established superconducting strand suppliers.

This manuscript was submitted to Superconductor Science & Technology (IOP) for possible publication
This manuscript was published by Superconductor Science & Technology (SuST, IOP) 27, No. 4, 044001, (2014).

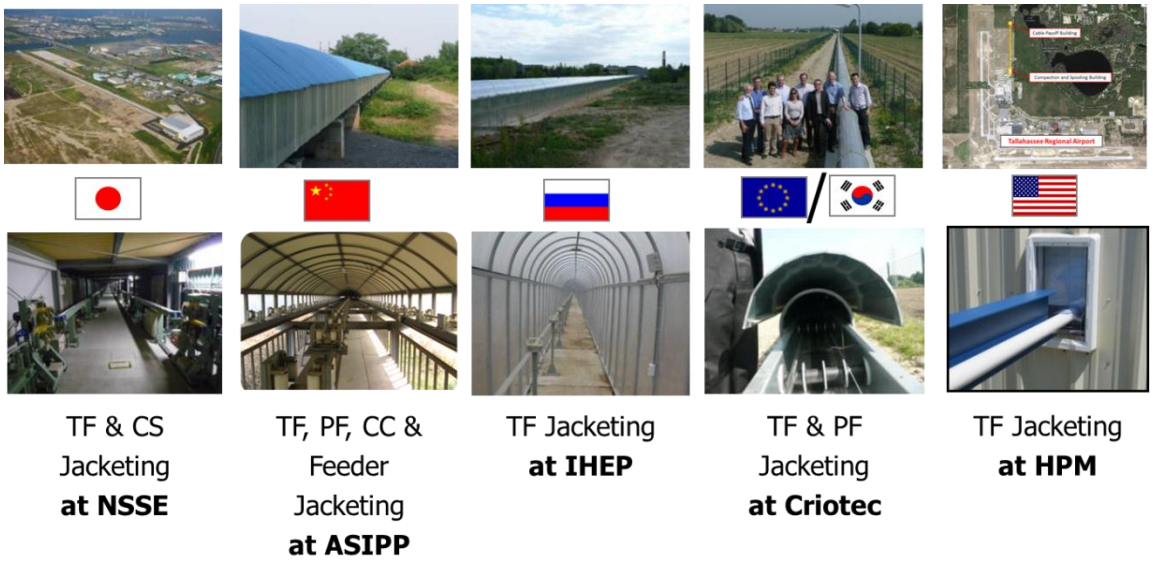

Figure 8: ITER jacketing lines around the world.

One particularity of ITER conductor manufacture is that it requires dedicated 800-1000 m long jacketing lines where to store the welded jacket assemblies and to carry out cable insertion prior to compaction and spooling. The feasibility of the jacketing concept for long length CICCs was first demonstrated in the mid 1990's in RF [36]. Five out of the six DAs involved in ITER conductor production have decided to set up their own jacketing line (namely: CN, EU, JA, RF and US), while KO has decided to subcontract its jacketing work to the EU supplier. Figure 8 shows pictures of the 5 jacketing lines. The one in Japan (located at NSSE in Kita-Kyushu) is rather spacious and can be biked along [37]. The one in China (located at ASIPP in Hefei), is more shallow and would require to crawl. The one in Russia (located at IHEP in Protvino) is of greenhouse type [21]. The one in Europe (used for both EU and KO productions and located at Criotec near Chivasso, Italy) is quite compact [38]. The one in the US (located at HPM in Tallahassee, Florida) is the most particular as it runs parallel to the Tallahassee airport runway. Save for the facility in Europe, which is used for both ITER and JT60 super upgrade conductor productions [39], all the other lines have been set up and are operated for ITER.

Given the large number of partners involved, it is critical to ensure standardization and uniformity of conductor production around the world. To do so, the 11 conductor PAs define detailed Quality Assurance (QA) and Quality Control (QC) requirements to be implemented by the DAs and their suppliers. Among others, these QA/QC requirements call for

- qualification and certification of manufacturing and test procedures (*e.g.*, orbital welding of jacket sections, local and global He leak tests),
- Statistical Process Control (SPC) on critical parameters,
- benchmarking of cryogenic test facilities,
- systematic low-temperature measurements on strands (critical current, hysteresis loss, residual resistivity ratio): head/tail of every billet + statistical sampling of breakages,
- regular low-temperature measurements on full-size conductors: 25% of TF conductor Unit Lengths (ULs), 10% of PF conductor ULs, 25% of CS conductor ULs.

This manuscript was submitted to Superconductor Science & Technology (IOP) for possible publication
This manuscript was published by Superconductor Science & Technology (SuST, IOP) 27, No. 4, 044001, (2014).

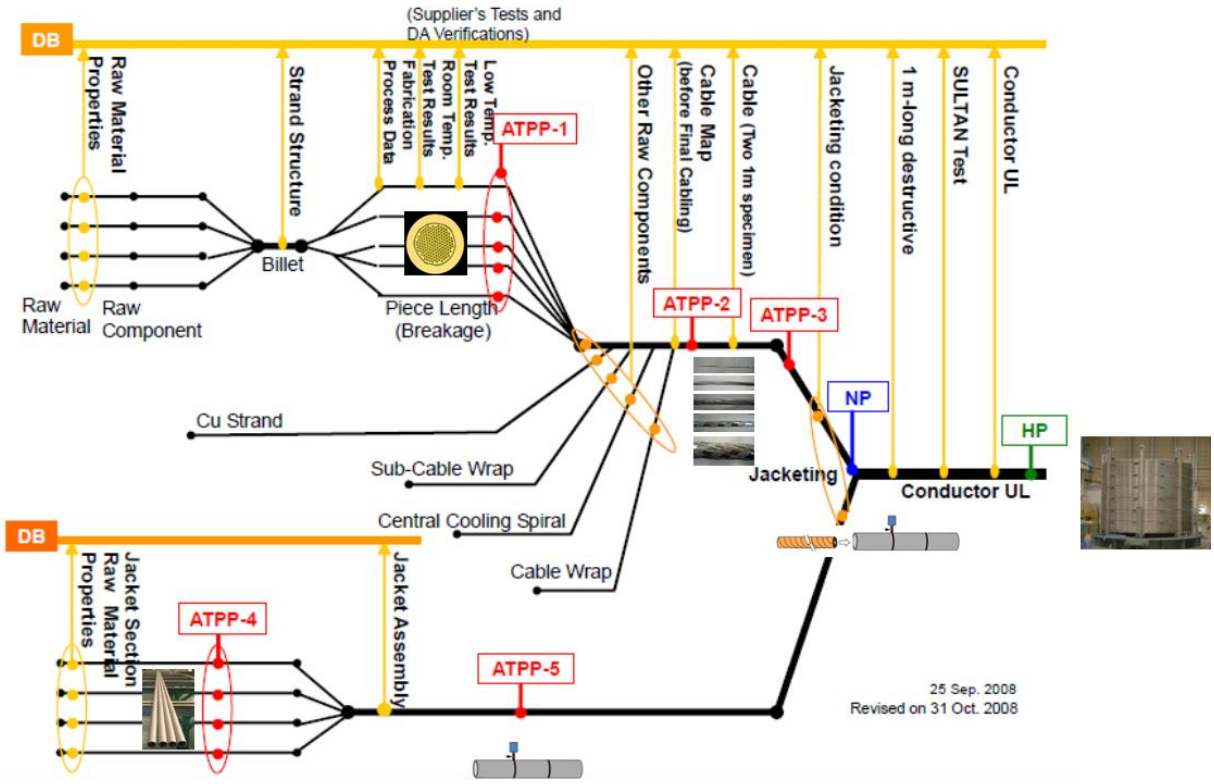

Figure 9: Control points of ITER conductor PAs and business flow of ITER Conductor Database (courtesy of K. Seo, ITER-IO).

In addition, as illustrated in Figure 9, the PAs define a number of control points where the suppliers and the DAs must seek clearance before proceeding to the next step. In total there are 7 seven control points: 5 authorizations to proceed (strand lot, cable map, cable, jacket section lot, and jacket assembly), one notification point (jacketing) and one hold point (final conductor). A strand lot is defined as all the strand unit lengths issued from the same multifilament billet, while a jacket section lot is defined as all the jacket sections issued from a same mother and ESR that have been processed at the same time down to the last solution annealing treatment.

The monitoring of the PA execution is ensured by means of a web-based Conductor Database, developed by the IO and used by the DAs and their suppliers worldwide [40]. The implementation of the conductor dataset, which ensures strict confidentiality of the DAs and individual supplier data has been quite successful. Presently, there are ~20 suppliers/DAs and ~150 users registered to input and verify data. Over the course of the last 4 years, the IO has cleared ~6900 control points, which, for the strand lots, rely on ~27,000 critical current measurements.

This manuscript was submitted to Superconductor Science & Technology (IOP) for possible publication
This manuscript was published by Superconductor Science & Technology (SuST, IOP) 27, No. 4, 044001, (2014).

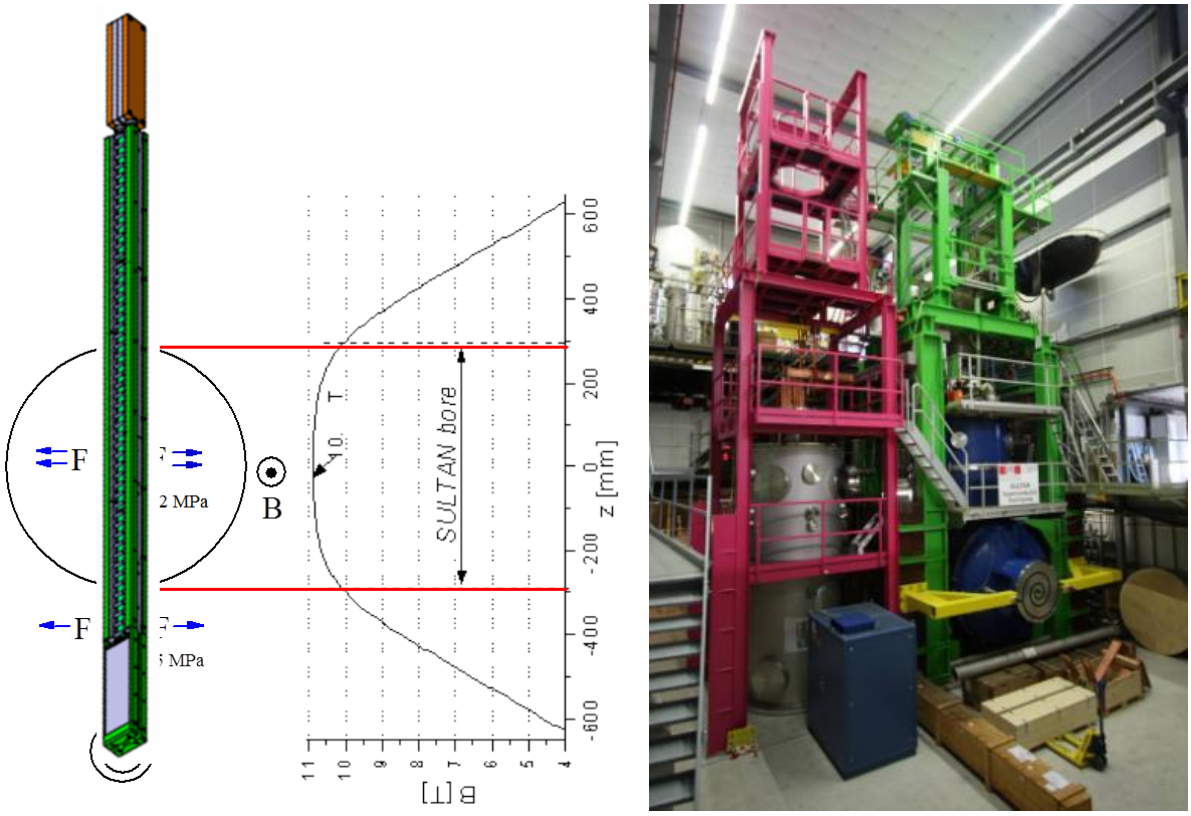

Figure 10: View of SULTAN sample test facility at CRPP (right) and SULTAN sample configuration (left; courtesy of P. Bruzzone, CRPP)..

The most difficult and critical acceptance tests are the full-size conductor tests which are carried out at the SULTAN facility, located in Villigen, Switzerland [41]. As illustrated in Figure 10, SULTAN samples are 3.6 m long, with a High Field Zone (HFZ) of ~400 mm (of the order of the last-stage cable twist pitch). Samples are tested in pairs with joints at the top and bottom (save for the Nb–Ti samples, which do not rely on a bottom joint but are tested in a hairpin configuration) and are instrumented with voltage taps and temperature sensors. Measurements are carried out either at fixed temperature and field, by increasing the transport current (I_C run) or at fixed current and field, by increasing the temperature (T_{Cs} run). The T_{Cs} runs are the ones used to assess the conductor performance.

4. Technical Challenges

Let us now illustrate some of the technical challenges encountered in the development and the production of ITER conductors.

4.1 Twist Pitch Elongation

As illustrated in Figure 11, during insertion into the jacket assembly, the rope-type cable head exhibits a tendency to rotate under the action of the pulling force. The number of rotations can be measured using a dedicated device, mounted between the cable head and the pulling wire, like the one developed by HPM in the USA, that relies on an accelerometer chip measuring gravity in the directions perpendicular and parallel to the chip face [42]. Figure 12 presents plots of accumulated number of rotations versus pulling force as recorded during the insertion of 415 m and 760 m TF cables at Criotec and HPM. It shows that the number of rotations can be up to 130.

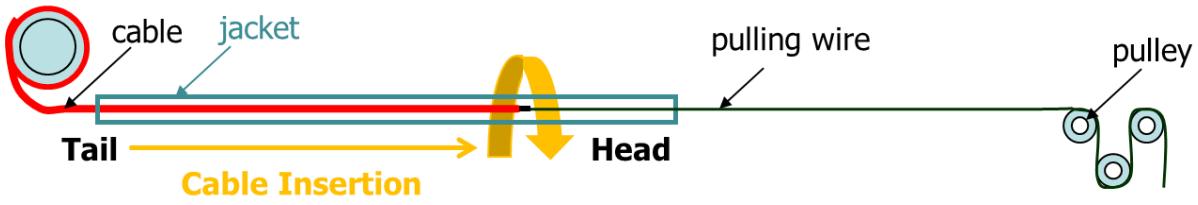

Figure 11: Principle of cable insertion into jacket assembly.

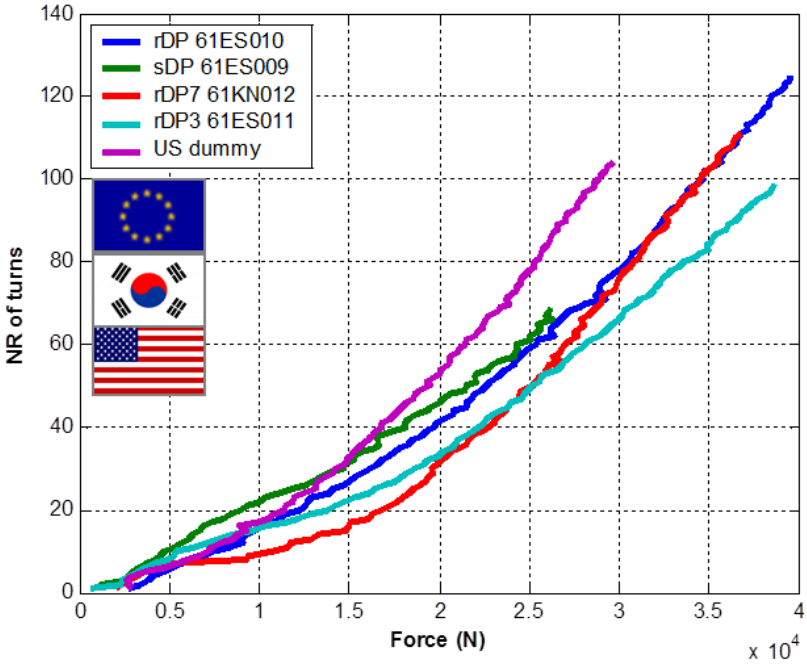

Figure 12: Accumulated number of cable head rotations versus pulling force, as recorded during insertion of TF RF cables at Criotec and HPM.

The cable rotation results in an elongation of the last stage twist pitch of the cable. The twist pitch elongation was confirmed by careful analyses carried out at the Japan Atomic Energy Agency (JAEA, the Japanese Domestic Agency) of laser diameter measurements performed on conductor jacket after compaction [43]. The measurements reveal a weak periodic pattern that is an imprint of the cable twisting. Figure 13 shows a plot of last stage cable twist pitch versus distance from cable head as estimated from laser diameter measurements recorded during the jacketing of a 760 m TF conductor unit length at NSSE. At the tail of the conductor, the twist pitch is 420 mm and it appears to increase gradually along the unit length to reach 470 mm at the conductor head. This high twist pitch value was confirmed by a direct measurement on a destructive examination sample that was cut at the conductor head and for which the last stage cable twist pitch was found to be 475 m. In comparison, the technical requirement for the last stage twist pitch is: 420 mm +/- 20 mm.

Such twist pitch elongation, well known to sailors using rope-type cables, is unavoidable. It can be up to 15%. As long as it is gradual along the cable unit length, it is not expected to significantly affect conductor performance and AC losses, in particular for the TF coils which are operated in a steady state. The main issue will be in the joints which should be designed to enable good current transfer out of the six 4th stage petals. The present plan is that the coil manufacturer will re-twist the cable as part of the joint manufacturing procedure.

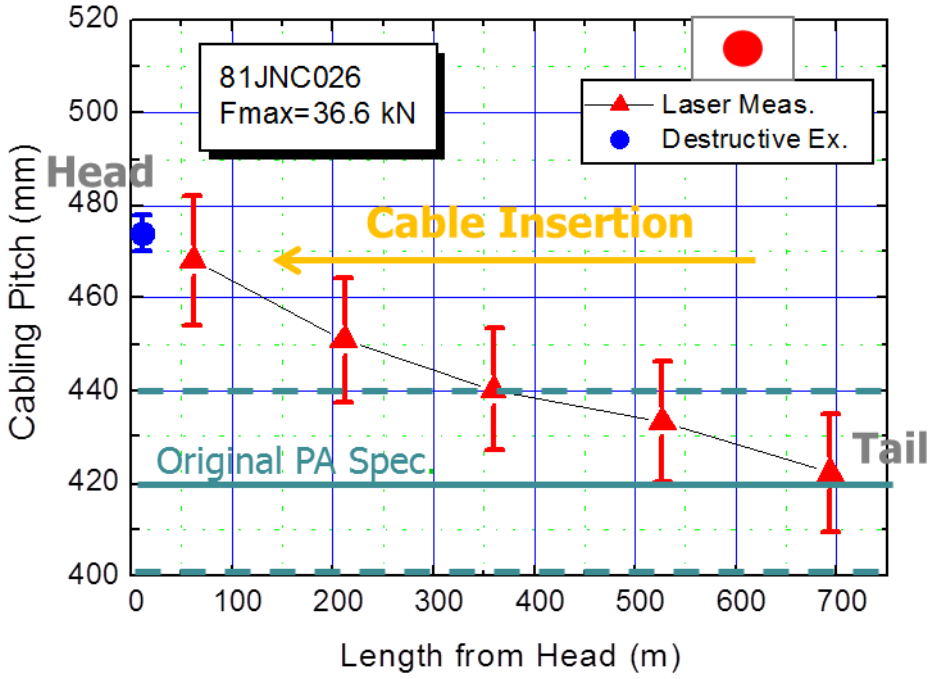

Figure 13: Distribution of last cable stage twist pitch along a 760 m TF conductor unit length manufactured at NSSE estimated from laser diameter measurements (red triangles) and from a destructive examination sample (blue circle; courtesy of Y. Takahashi, JAEA).

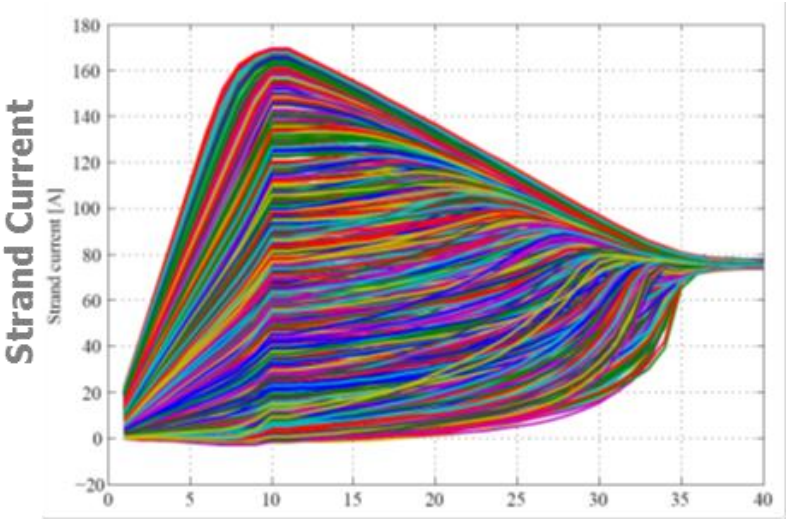

Figure 14: Numerical simulation (using the Jackpot code) of current distribution evolution during a current ramp to nominal current followed by a temperature ramp as in a T_{Cs} run on a TF conductor sample at SULTAN (courtesy of E.V. van Lanen, Twente University).

4.2 SULTAN Samples

4.2.1 SULTAN Sample Issues

SULTAN is the only facility in the world where full size, ITER-type CICCs can be tested. The preparation, instrumentation and representativity of SULTAN samples have been the object of many debates within the community. The main issues that have been singled out over the years are:

- For Nb_3Sn samples, how to control and even prevent cable/jacket slippage at the sample extremities that may arise as a result of thermal shrinkage differential between 650 °C and 4.2 K [44] (the integrated thermal shrinkage of Nb_3Sn is estimated to be -0.9% while that of stainless steel is estimated to be -1.5% [45]) and how to ensure that the sample is in a reproducible and representative strain state (compressive for the cable and tensile for the jacket)?
- For all samples and given the large number of strands in the cable (900 superconducting strands in the case of TF), how to ensure good current distribution among cable strands and prevent large current imbalances like the ones depicted in Figure 14 [46]?
- How to best assess average sample voltages and temperatures?
- Are the results of SULTAN samples (where a short High Field Zone is in close proximity to joints) representative of in-coil performance?

This manuscript was submitted to Superconductor Science & Technology (IOP) for possible publication
This manuscript was published by Superconductor Science & Technology (SuST, IOP) 27, No. 4, 044001, (2014).

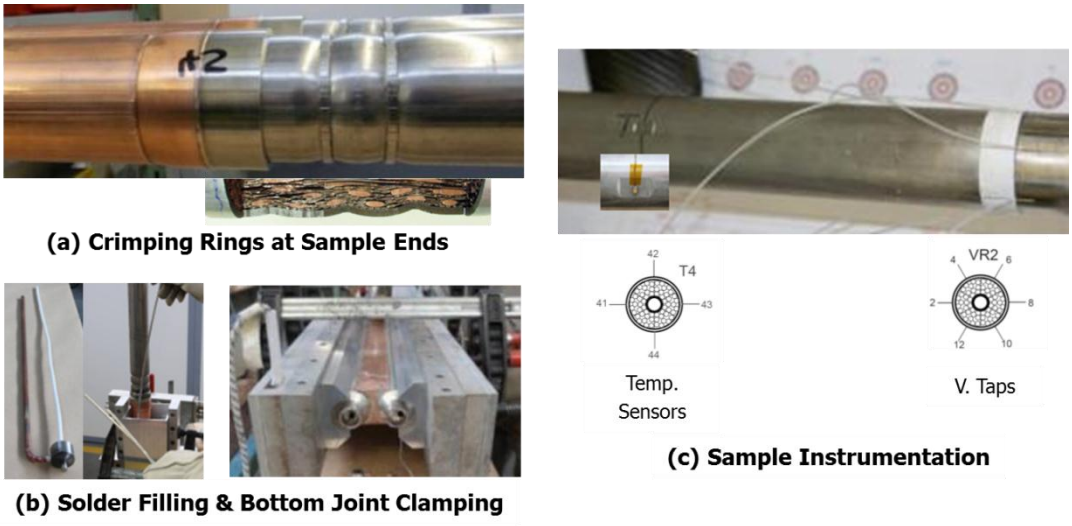

Figure 15: Improvements implemented in the preparation/instrumentation of SULTAN samples at CRPP (Courtesy of P. Bruzzone, CRPP).

In 2007 and 2008, ITER IO funded several contracts at CRPP to improve SULTAN sample preparation and address the above issues. The final procedure, agreed with all six domestic agencies involved in conductor production, and which is used for qualification and production samples, includes [47]

- 2 sets of crimping rings at both ends of the sample (to prevent cable/jacket slippage; see Figure 15a) [48],
- solder-filled joints for both the bottom joint and the upper terminations (to ensure good current uniformity among cable strands; see Figure 15b) [49-50],
- crown arrays of 6 voltage taps and 4 temperature sensors mounted on the conductor jacket and on both sides of the High Field Zone (which have been shown by analyses to best approximate average cable properties; see Figure 15c) [51].

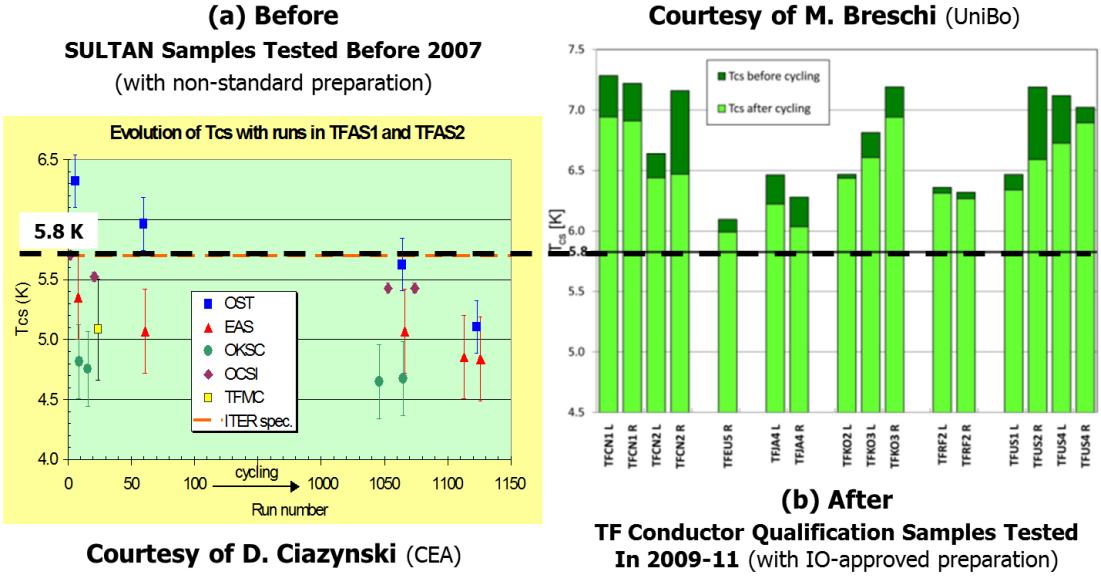

Figure 16: results of T_{CS} measurements on ITER conductor samples at SULTAN before (a) and after (b) implementation of improvements in sample preparation and instrumentation.

The results of these improvements are clearly illustrated in Figures 16(a) and (b) which display the results of T_{Cs} runs carried out on 2 sets of full-size, Nb_3Sn conductor samples for ITER: one set tested before (16a) [52] and one set tested after (16b) the final preparation procedure was implemented. The samples presented in Figure 16(b) correspond to the TF Conductor Performance Qualification Samples (CPQS) that each DA was required to manufacture and test to qualify potential suppliers prior to contract award and launch of production [47]. All CPQSs met the acceptance criterion for TF conductors defined as: T_{Cs} (at 10 μV/m) greater than 5.8 K after 1000 electromagnetic (EM) cycles to 68 kA in a SULTAN background field of 10.78 T (corresponding to a conductor peak field of 11.8 T and an effective field of 11.3 T).

4.2.2 SULTAN Sample Summary

Since 2009, a number of TF conductor production samples have been tested, making it to gather statistics for both Internal Tin (IT) and bronze conductors and to look for possible trends.

Figure 17(a) presents a summary of the T_{Cs} data obtained for the 3 productions of conductors relying on IT strands in CN [16], EU [53-54] and KO [55-56]. All IT TF conductor samples show good performance, with a significant margin above 5.8 K after 1000 EM cycles.

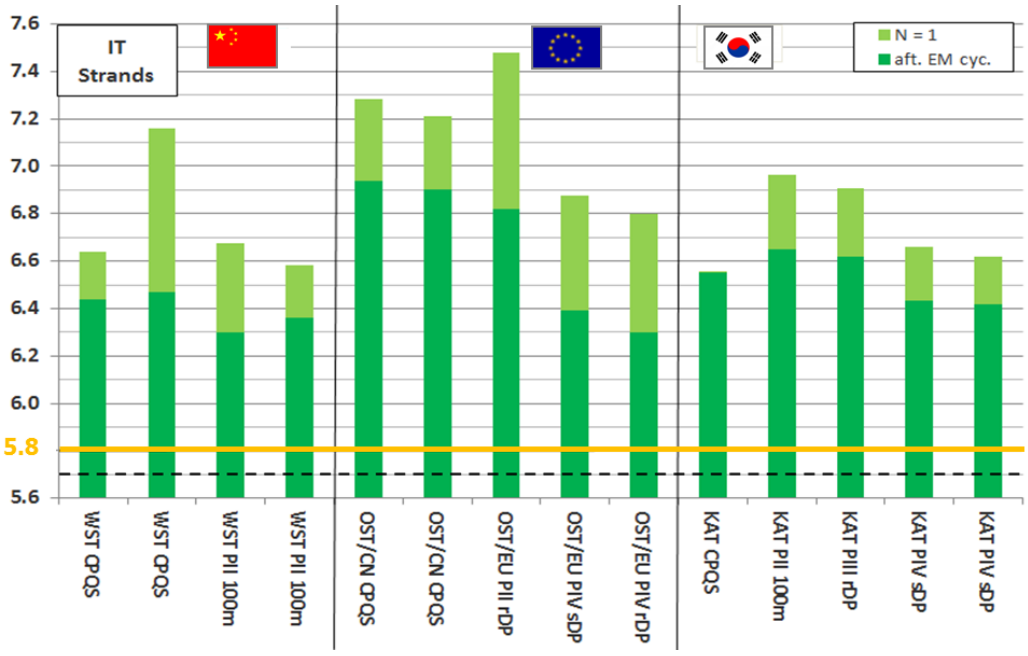

This manuscript was submitted to Superconductor Science & Technology (IOP) for possible publication
This manuscript was published by Superconductor Science & Technology (SuST, IOP) 27, No. 4, 044001, (2014).

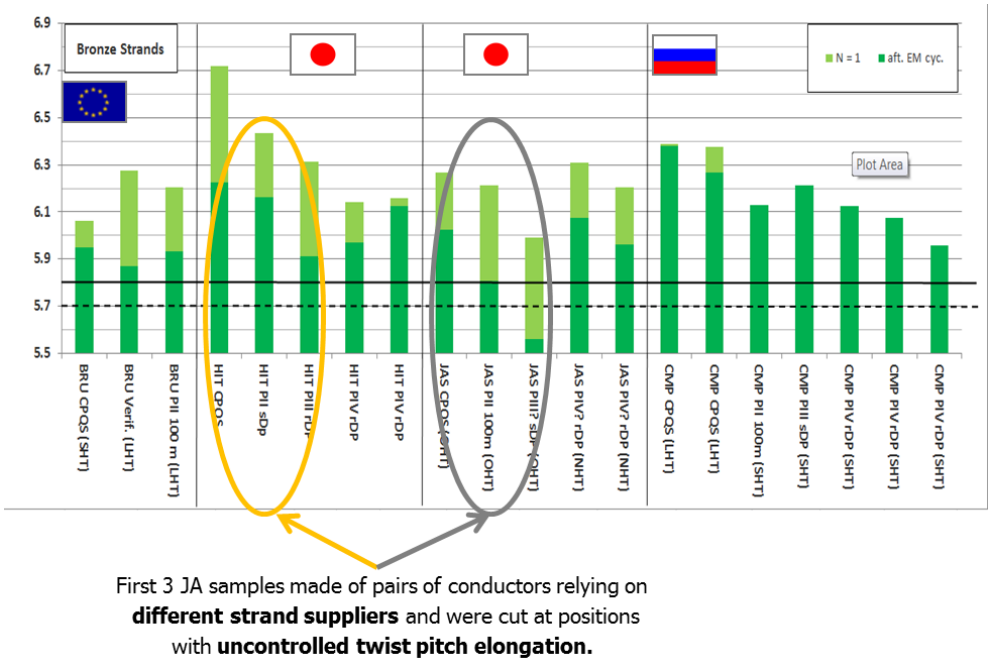

Figure 17: results of T_{Cs} measurements on ITER TF conductor production samples: (a) conductor relying on IT strands (top) and (b) conductor relying on bronze strands (bottom).

Figure 17(b) presents a similar plot for the conductor productions relying on bronze strands. In this case, all samples but one met the 5.8 K after 1000 EM cycles. Looking at the details of the results, it appears that all RF samples show good performance with no cycling degradation (there is even usually a small increase of T_{Cs} over the first 50 to 100 EM cycles, the origin of which will be discussed later) [57-58]. The EU samples are reproducible, but appear very close to the limit after EM cycling (this particular conductor design was optimized to perform in such fashion) [54]. The first 3 sets of data from the 2 JA suppliers show irregular performance (there even appears to be a degradation from sample to sample) [59-60]. There are two peculiar facts regarding these samples: 1) unlike all the other samples presented in Figure 17, the first 3 JA samples were made of pairs of conductors relying on strands from different suppliers (one leg from strand supplier 1, the other leg from strand supplier 2) and 2) the samples were cut at the head of the conductors after compaction at a time when the issue of twist pitch elongation described in section 5.1 had not yet been identified. Therefore, they were cut in a region of uncontrolled variations of last stage twist pitch. Since then, JA has tested 2 more samples which are made of conductor pairs relying on the same strand supplier (2 legs from either strand supplier 1 or strand supplier 2) and were cut in a region where the last stage twist pitch is under control. As seen in Figure 17(b), both samples were successful and met the 5.8 K criterion after 1000 EM cycles with a margin comparable to that of the RF samples (although, in the JA case, the conductors do exhibit cycling degradation). These results seem to confirm that the erratic behaviour of the earlier samples was likely due to a sample problem rather than a conductor problem. Let us note that the JA conductor corresponding to the sample leg that did not meet the acceptance criterion has been set aside and will be used for winding trials by one of the JA coil manufacturers.

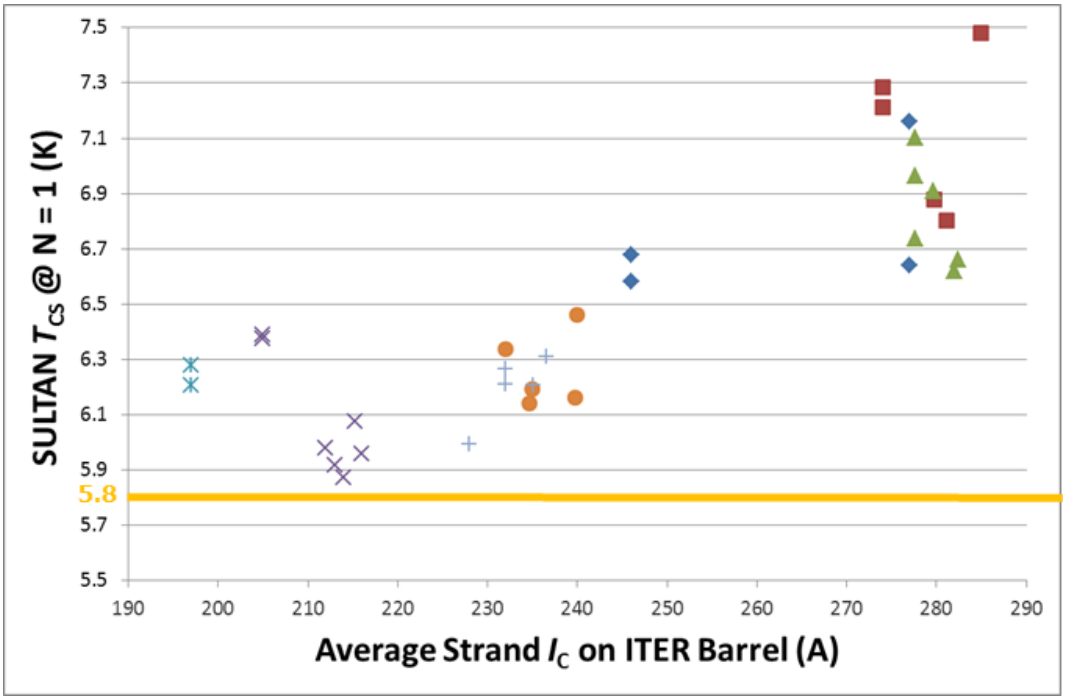

Figure 18: Correlation plot of T_{Cs} (at 68 kA and 10.78 T background field) assessed during first energization cycle vs. average strand I_C (at 4.2 K and 12 T) on ITER barrel for ITER TF conductor production SULTAN samples.

4.2.3 Correlation with Nb_3Sn Strand Performance

A longstanding question has been whether or not the performance of a Nb_3Sn CICC sample tested in SULTAN could be related to the performance of its strands. In the past, all attempts at finding such correlation failed, leading to a flurry of papers and interpretations. The ITER TF conductor production offers the unique opportunity of looking at a data set on a series of samples prepared in the same manner and cut from conductors manufactured in a reproducible way. Figure 18 shows a plot of T_{Cs} measured during the first energization after cooldown at 68 kA and 10.78 T (background field) for selected ITER TF conductor samples versus the average critical current, I_C, of their strands measured at 4.22 K and 12 T (on so called "ITER barrel") as part of QC tests during production (the ITER barrel was introduced in the mid-1990s in an effort to standardize strand critical current measurements.) The data are not randomly distributed and there appears to be a correlation.

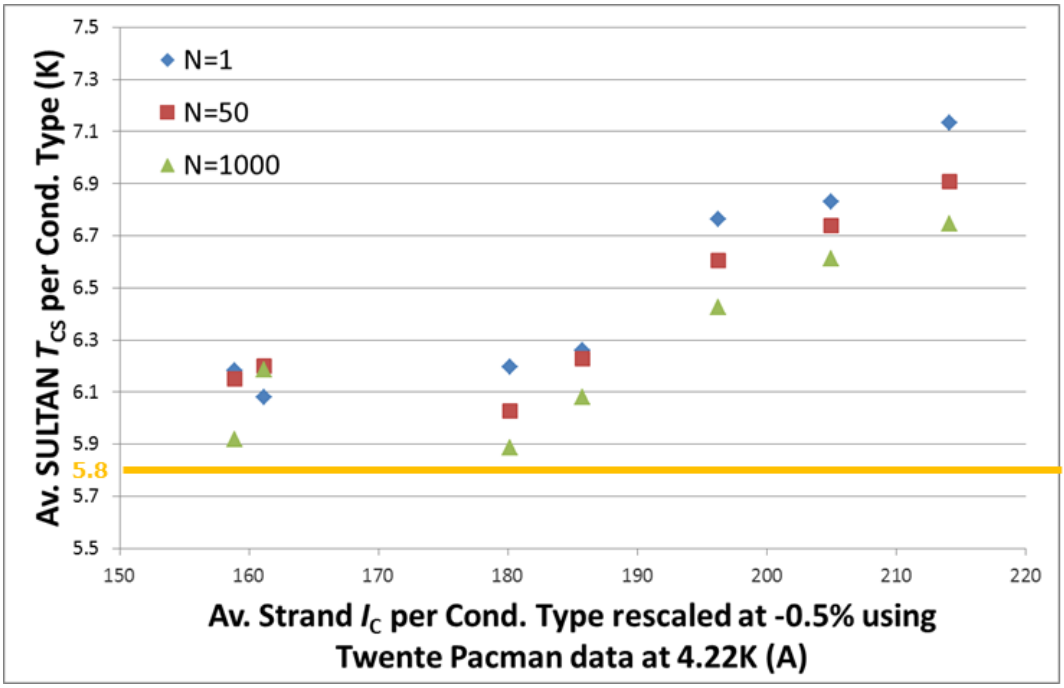

Figure 19: Correlation plot of average T_{Cs} (at 68 kA and 10.78 T background field) per ITER TF conductor/strand type assessed for 1st, 50th and 1000th energization cycle vs. rescaled average strand I_C (at 4.2 K, 12 T and about -0.5% strain) using slope of I_C versus strain curve measured for each strand type on pacman set up at Twente University.

The correlation can be further improved by applying a correction to the I_C data. Indeed, when measured on ITER barrel, the strands are more or less unconstrained, and the Nb_3Sn filaments only experience the intrinsic compressive strain arising from the thermal shrinkage differentials between the filaments and the other materials constitutive of the strands. This intrinsic strain is usually estimated in the range of -0.15 to -0.25% [45, 61]. In a CICC, this intrinsic strain is augmented by the strain applied by the stainless steel jacket, whose integrated thermal shrinkage between 650 °C and 4.2 K is larger than that of Nb_3Sn (see section 5.2.1) to reach a value of the order of -0.5% (see section 4.3.5). ITER IO has placed a contract with Twente University to fully characterize the I_C versus strain dependency of all ITER strand types [62]. The Twente measurements are carried out on a pacman test set up and enable an assessment of the slope of the I_C versus strain degradation on the compressive side which is usually linear. The slope appears to vary by a factor of 2 depending on the strand type. Figure 19 shows the same data as in Figure 16, but in average of each conductor/strand type and with a rescaling of the I_C data to a strain of -0.5% using the slope assessed by Twente University for each strand type. In addition, Figure 19 shows the T_{Cs} results for cycle 1, cycle 50 and for the last cycle (usually 1000). This time and in spite of the crude correction that is applied, there appears a clear correlation between the average T_{Cs} of the SULTAN samples and the re-scaled average I_C of their strands.

4.2.4 Correlation with In-Coil Performance

The consistency of the results presented above provides strong evidence that SULTAN can be used for QC testing of CICCs as foreseen in the procurement arrangements for the ITER conductors. A last question is whether or not SULTAN test results are representative of in-coil performance. In particular, there are some concerns that the sample configuration and the short high field zone result in strain distributions and/or strain relaxations along the conductor sample leg that affect the T_{Cs} and that would not occur in a real coil configuration [63, 64]

This issue will be assessed by the manufacture of a new Central Solenoid Insert (CSI) coil to be tested at the Central Solenoid Model Coil (CSMC) facility in Naka [65], Japan and by the manufacture and test of a matching SULTAN sample, cut from the same conductor unit length. The new CSI has been designed by the US-ITER Project Office (US-IPO) [66] and is being manufactured in Japan under the supervision of JAEA. Cold test is foreseen in 2014/15. The motivation for this new CSI test is twofold:

1) to determine the ultimate performance of the CS conductor in a real coil configuration, taking into consideration the effects of the hoop strain (up to +0.17% in the second coil module from the top of the stack, referred to as CS2U),
2) to compare the results of the CSI test with those of the matching SULTAN sample (where the hoop strain effects cannot be simulated). Note that this is the first time that an ITER model coil test will be accompanied by a matching SULTAN sample test.

4.3 CS Conductor Degradation

4.3.1 CS Coil Requirements

As already explained, the CS coil is made up of 6 modules which are independently powered. Unlike the TF coils, which are operated in a steady state, the CS and PF coils must be capable of driving inductively 30,000 15 MA plasma pulses with a burn duration of 400 s [4,22]. This implies that during their lifetime, the CS coil modules will have to sustain severe and repeated electromagnetic (EM) cycles to high current and field conditions, which are way beyond anything large Nb_3Sn coils have ever experienced.

The CS conductor qualification program calls for the manufacture and test of SULTAN samples to be subjected to a large number of EM cycles (*e.g.*, 10,000). The expectation from the ITER model coil test program, in particular, the first CS Insert coil tested in the CSMC in Naka in 2000, is that the conductor performance should achieve stabilization after a few thousand EM cycles [67-68].

This manuscript was submitted to Superconductor Science & Technology (IOP) for possible publication
This manuscript was published by Superconductor Science & Technology (SuST, IOP) 27, No. 4, 044001, (2014).

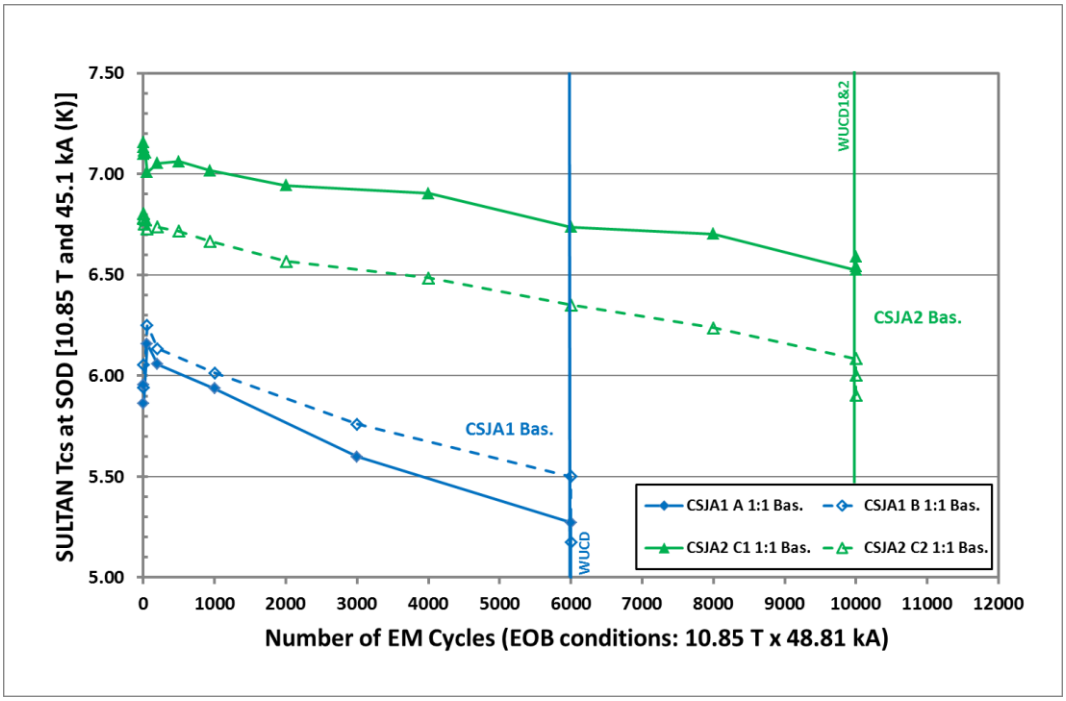

Figure 20: Summary plot of T_{CS} vs. EM and thermal cycling measured on first set of CS conductor qualification samples prepared under the supervision of JAEA (CSJA1 and CSJA2).

4.3.2 Early JA Samples

In 2010 and 11, JAEA tested 2 CS conductor qualification samples referred to as CSJA1 and CSJA2. CSJA1 relies on 2nd generation bronze strands from 2 suppliers similar to those used for the TF production [32], whereas CSJA2 relies on a new (3rd) generation of bronze strands from a 3rd supplier, with non-copper critical current densities in excess of 1000 A/mm^2 at 4.2 K and 12 T (on ITER barrel) [69].

As illustrated in Figure 20, which shows plots of T_{Cs} versus number of cycles for the four legs of CSJA1 and CSJA2, the performance of CSJA1 was unacceptable, whereas that of CSJA2, although much better, did not exhibit any tendency to saturate [53,70].

An autopsy of CSJA1 carried out by JAEA enabled 2 critical observations [70]:

1) in the high field zone of the sample, which was subjected to high Lorentz forces, the cable appears to have been permanently displaced inside the conduit (see Figure 21(a))
2) the non-compressive side of the high field zone cable shows evidences of strand buckling and even cracking (see Figure 21(b)).

These observations provided clear indications that the conductor design used for these samples was not appropriate for this application.

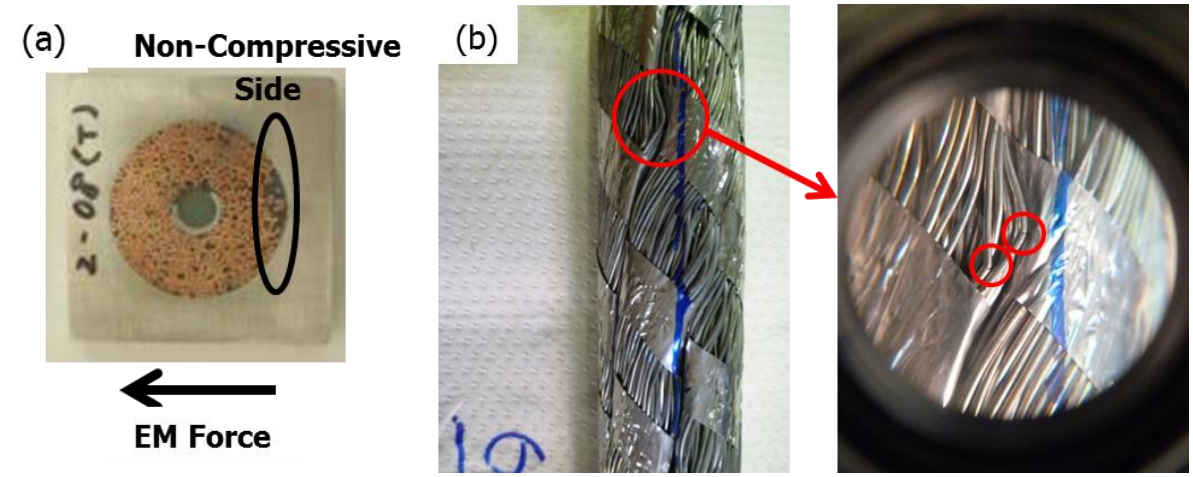

Figure 21: Pictures from the autopsy of CSJA1 at JAEA showing: (a) evidence of global displacement of cable inside conduit under the effect of the Lorenz force (left) and (b) evidence of strand buckling/cracking on the non-compressive side of the high field zone section (right; courtesy of Y. Takahashi, JAEA).

4.3.3 IO Crash Program

In the spring of 2010, ITER-IO launched, with support from US-IPO (US ITER Project Office) and OST, a comprehensive crash program to investigate different CS strand/cable configurations so as to achieve more robust performance as a function of electromagnetic and thermal cycling [22]. The program was aimed at assessing

- internal tin versus bronze strand designs [22],
- the effect of copper segregation, by comparing baseline cable inner triplet design with (2x1:1 sc + 1xCu) strands [15] vs. ITER model coil triplet design with (3x1.5:1 sc) strands [71-72],
- the effect of cable twist pitch sequence, by comparing short [73-74], versus baseline [15], versus pseudo long twist pitches [75].

This led to the manufacture of 4 types of conductors and 2 SULTAN samples, referred to as CSIO1 and CSIO2 [22]. Table 1 summarizes salient parameters of these conductors/samples. It should be noted that it is the first time in the ITER history that such a systematic R&D program, where only one parameter is changed at a time, was carried out.

Figure 22 shows plots of T_{Cs} versus number of cycles for the four legs of the CSIO samples. Three of the legs (CSIO1 1.5:1, CSIO1 1:1 and CSIO2 PLTP) exhibit a more or less similar degradation as a function of EM and thermal cycling, while the remaining leg, CSIO2 STP, exhibits a fundamentally different behavior: its T_{Cs} does not degrade, on the contrary, it keeps increasing slightly as a function of both EM and thermal cycling. The CSIO2 STP conductor relies on IT strands, a baseline (2x1:1 sc + 1xCu) inner triplet, short twist pitches and tight compaction and was the first conductor sample to pass the SULTAN test qualification for CS conductors. The use of short twist pitches has been advocated by CEA since the early 1990s [74] and the twist pitch sequence used in CSIO2 STP is similar to the sequence used in the inner layer (1.1) of the CS Model Coil manufactured and tested in the late 1990s [73].

Table 1: Salient Parameters of CSIO conductors.

	Baseline PA Requirements	CSIO1 Left Leg (1.5:1)	CSIO1 Right Leg (1:1, ~Baseline)	CSIO2 Left Leg (STP)	CSIO2 Right Leg (PLTP)
Strand					
Type	CS	IT	ITER TF/IT	ITER TF/IT	ITER TF/IT
Diameter (mm)	0.830 ± 0.005	0.82	0.82	0.822-0.823	0.822-0.823
Cu:non-Cu ratio	1.0:1	1.5:1	1.0:1	0.94-0.95	0.94-0.95
I_c at 12 T, 4.2 K on ITER barrel (A)	≥ 220	223-226	263-274	266-274	266-274
Cable	(2 sc + 1 Cu)	(3 sc)	(2 sc + 1 Cu)	(2 sc + 1 Cu)	(2 sc + 1 Cu)
Layout	x3x4x4x6	x3x4x4x6	x3x4x4x6	x3x4x4x6	x3x4x4x6
Stage 1 twist pitch (mm)	45 ± 5	45	45	22 [a)]	110 [a)]
Stage 2 twist pitch (mm)	85 ± 10	83	83	45 [a)]	115 [a)]
Stage 3 twist pitch (mm)	145 ± 10	141	141	81 [a)]	127 [a)]
Stage 4 twist pitch (mm)	250 ± 15	252	242	159 [a)]	140 [a)]
Stage 5 twist pitch (mm)	450 ± 20	423	423	443 [a)]	385 [a)]
Compacted Conductor					
Outer Dimensions (mm)	49.0x49.0	49.0x49.0	49.0x49.0	49.0x49.0 [a)]	48.3x48.3 [a)]
Jacket Inner Ø. (mm)	32.6	32.6	32.6	32.9 [a)]	31.8 [a)]
Void Fraction (%)		33.4	33.4	32.4 [a)]	29.1 [a)]

[a)] measured by destructive inspection of compacted conductor sample.

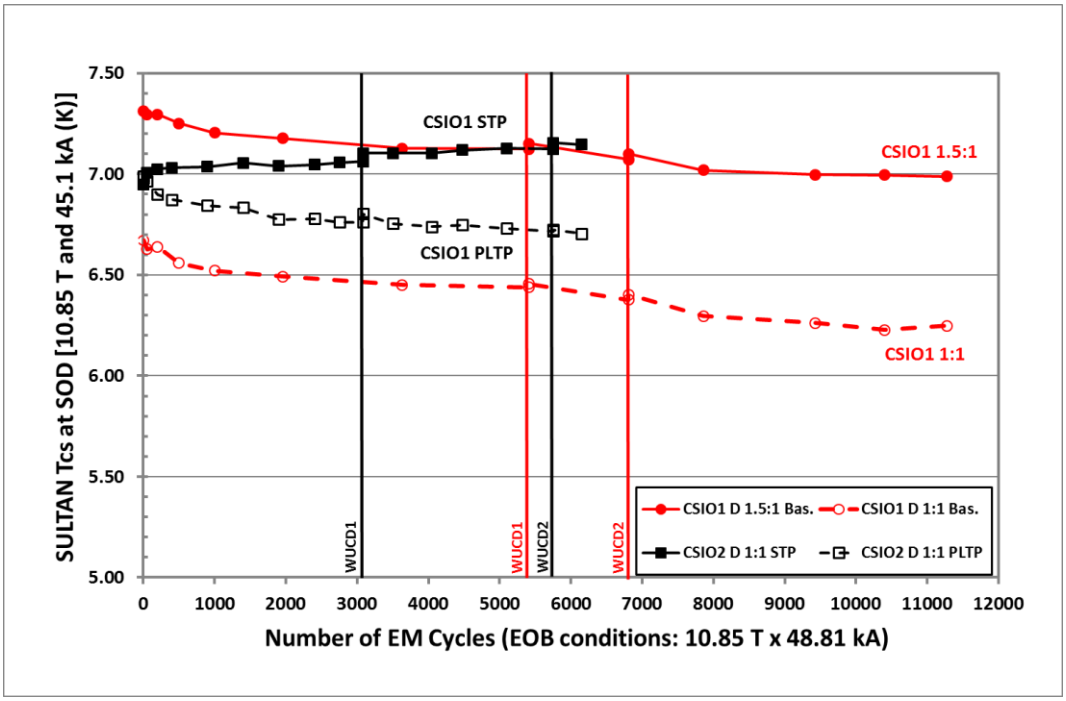

Figure 22: Summary plot of T_{CS} vs. EM and thermal cycling measured on CS conductor qualification samples prepared as part of the IO crash program (CSIO1 and CSIO2).

4.3.4 New JA Samples

Following up the success of the ITER-IO crash program, JAEA manufactured a new set of 2 SULTAN samples (4 legs), referred to as CSJA3 and CSJA5, relying on 3rd generation bronze strands from 3 different Japanese suppliers and short cable twist pitches/tight compaction similar to the successful leg of CSIO2 [76]. Figure 23 shows plots of T_{Cs} versus number of cycles for the four legs of CSJA3 and CSJA5, while Figure 24 shows a summary plot for all CS qualification samples tested up to date of ΔT_{Cs} versus number of cycles, where ΔT_{Cs} is the difference between the T_{Cs} at a given cycle number, N, and the T_{Cs} at $N = 1$.

This manuscript was submitted to Superconductor Science & Technology (IOP) for possible publication
This manuscript was published by Superconductor Science & Technology (SuST, IOP) 27, No. 4, 044001, (2014).

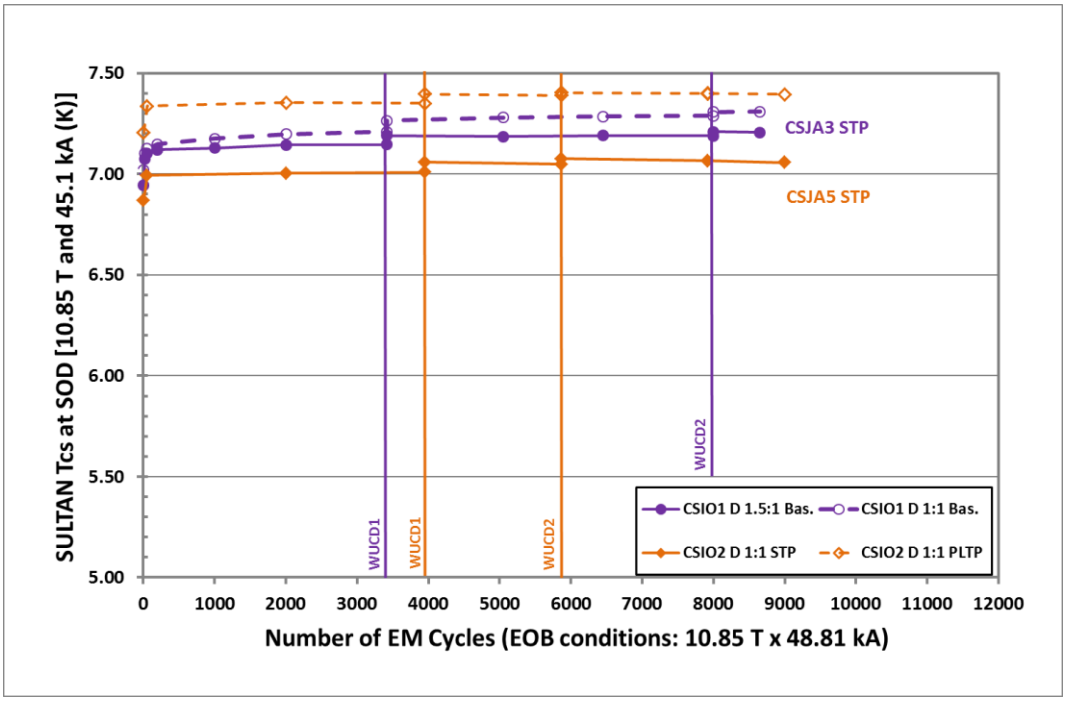

Figure 23: Summary plot of T_{CS} vs. EM and thermal cycling measured on second set of 2 CS conductor qualification samples prepared under the supervision of JAEA (CSJA3 and CSJA5).

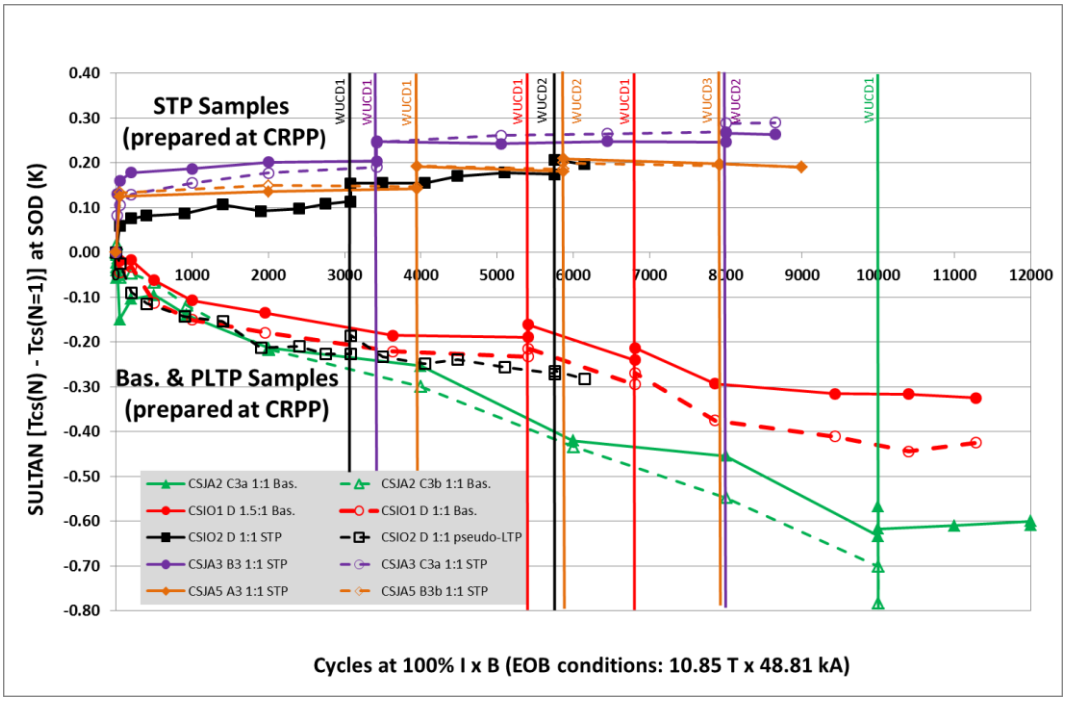

Figure 24: summary plot of ΔT_{Cs} versus number of cycles, where ΔT_{Cs} is the difference between the T_{Cs} at a given cycle number, N, and the T_{Cs} at N = 1, for all ITER CS qualification samples tested up to date.

Figure 24 clearly show that all STP conductor samples exhibit a similar behavior and pass the SULTAN test qualification with no degradation versus EM and thermal cycling. In fact, they all exhibit a slight T_{Cs} increase that shall be commented upon in section 4.3.6. These

successful tests enabled the qualification of four potential strand suppliers (one internal tin and three bronze) and the launch by JAEA of its calls for tender for the manufacture of the CS conductors. At present, contracts have been placed and production is underway for the conductors of the bottom module of the CS coil stack (referred to as CS3L).

4.3.5 Thermal Strain Assessment

The good performances of the short twist pitch samples are confirmed by assessments of thermal strain distributions over the cross-sections of the High Field Zones of SULTAN samples. The thermal strain is derived from magnetic susceptibility measurements carried out, in situ, as a function of temperature, at zero current and background field [77]. As illustrated in Figures 25a and b, the strain distribution assumes a bell-type shape which evolves with cycling. For most samples, such as the baseline leg of CSIO1 (see Figure 25a), the strain distribution flattens, which is a sign of degradation, and moves towards more compressive strains, which is consistent with the observed decrease in T_{cs} during EM cycling [78]. Such broadening of internal strain distribution was also observed by neutron diffraction technique when comparing data accumulated over a conductor volume corresponding to the non-compressive side of the High Field Zone of CSJA1 with those accumulated over a conductor volume in the Low Field Zone, that has not experienced the effect of the Lorentz forces [79]. However, in the case of the STP conductor samples, such as CSJA5 (see Figure 25b), the strain distribution does not deform, confirming the absence of degradation, and moves towards less compressive strains, which is consistent with the observed increase in T_{cs} during EM cycling [80].

Let us note that the bell shape distributions after cooldown presented in Figure 25 are centered around -0.5%. This is the justification for the value assumed in the rescaling of the I_C data in section 4.2.3 and Figure 19.

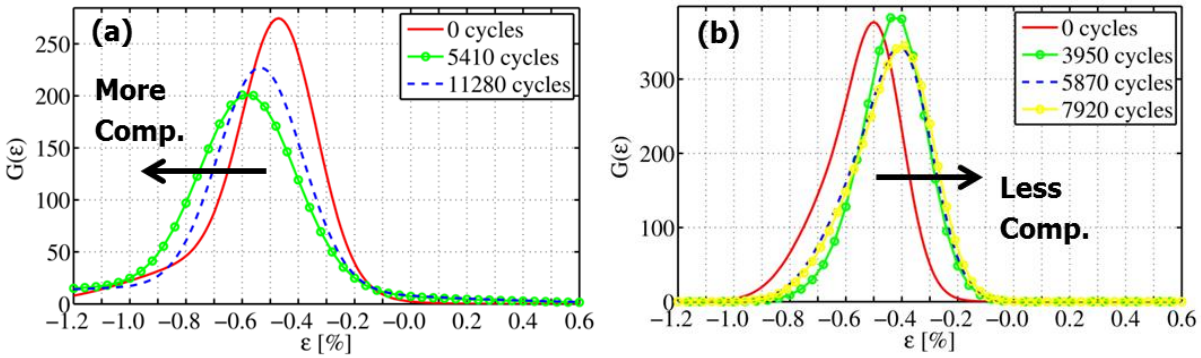

Figure 25: Evolution of the thermal strain distribution over the cross-section of the High Field zones of ITER CS conductor SULTAN samples as a function of EM cycling: (a) baseline leg of CSIO1 (left) and (b) CSJA5 STP (right; courtesy of C. Calzolaio, CRPP).

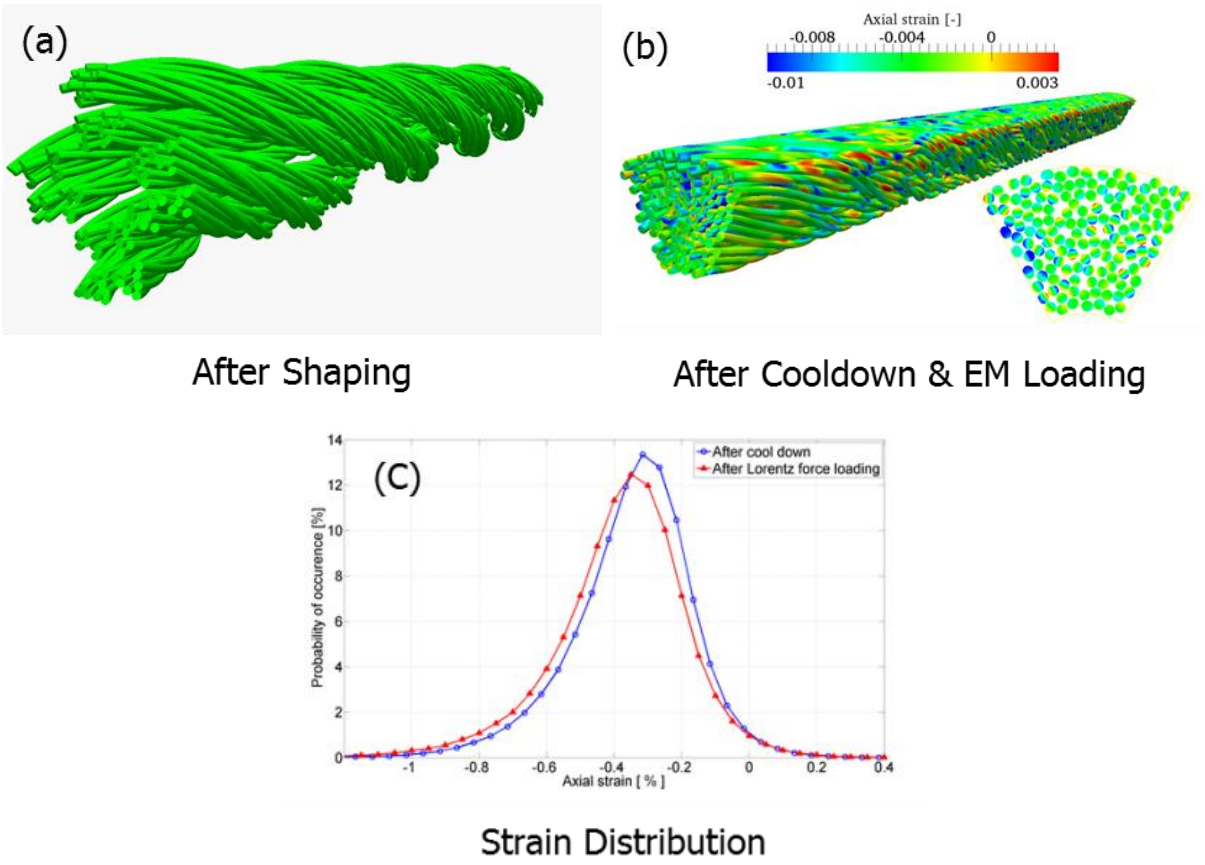

Figure 26: ITER CICC petal as modeled by the Mutltifil code (TF conductor): (a) after shaping, (b) after cooldown and electromagnetic loading and (c) strain distribution after cooldown and after cooldown and energization (Courtesy of D. Durville, ECP and H. Bajas, CERN).

4.3.6 Multifil Analyses

Many analyses have been carried out to predict and/or interpret the results of the CSIO samples with more or less success. Among them are numerical simulations with the Multifil code developed by Ecole Centrale Paris for ITER-IO and CEA [81-83]. As illustrated in Figures 26a, b and c, Multifil enables one to compute strain distributions in a petal of an ITER-type CICC as a function of shaping, cooldown and energization. The computed strain distributions assume bell-type shape with very long tails, both in tension and compression, similar to the ones described in section 5.2.5 (compare Figures 25 and 26(c)). These long tails are believed to play a dominant role in determining the conductor performance.

Figure 27a displays pure bending strain distributions as computed by Multifil for the various twist pitch sequences considered in the CSIO samples. It clearly appears that the STP option exhibits less propensity to bending than the Baseline and Pseudo-Long Twist Pitch (PLTP) options. This confirms that the short twist pitches and tight compaction are likely to provide better strand support, and, thereby, to prevent the deleterious bending and displacements at the origin of T_{Cs} degradation.

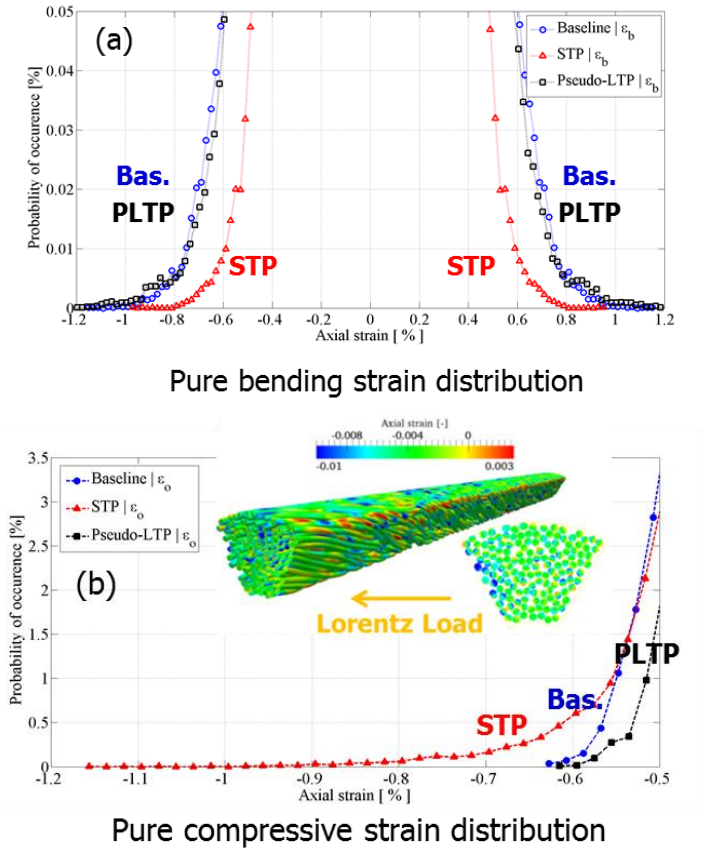

Figure 27: results of Multifil simulations for the 3 twist pitch sequences used in the CSIO samples (STP: short twist pithc, Bas.: Baseline, and PLTP: pseudo long twist pitches): (a) pure bending strain distribution (left) and (b) pure compressive strain distribution (right; courtesy of H. Bajas, CERN).

In addition, the Multifil simulations also show that the STP option exhibits the longest tail on the pure compressive side (see Figure 27b). Since, in the range of interest, the effects of compressive strain are reversible on the strand performance, one can speculate that compressive strain relaxation during EM/thermal cycling is the likely reason for the slight T_{CS} increase observed during testing in SULTAN. At this stage, it is not possible to conclude whether such compressive strain relaxation will also take place in a real coil configuration or if it is an artifact of SULTAN sample tests [63].

4.3.7 FSU Metallography

Over the last few years, Florida State University (FSU) has developed some amazing polishing, etching and imaging techniques that can be used to investigate strand deformation and filament fracture in ITER-type CICCs [84-86]. Figure 28 shows examples of such images, starting from a full CS conductor cross-section cut from the high field zone of a SULTAN sample after test completion (5 mm scale), followed by images of etched strands showing evidences of broken filaments (200 μm scale), and close up views of the broken filaments' facies showing the details of their grain structure (5 μm scale).

This manuscript was submitted to Superconductor Science & Technology (IOP) for possible publication
This manuscript was published by Superconductor Science & Technology (SuST, IOP) 27, No. 4, 044001, (2014).

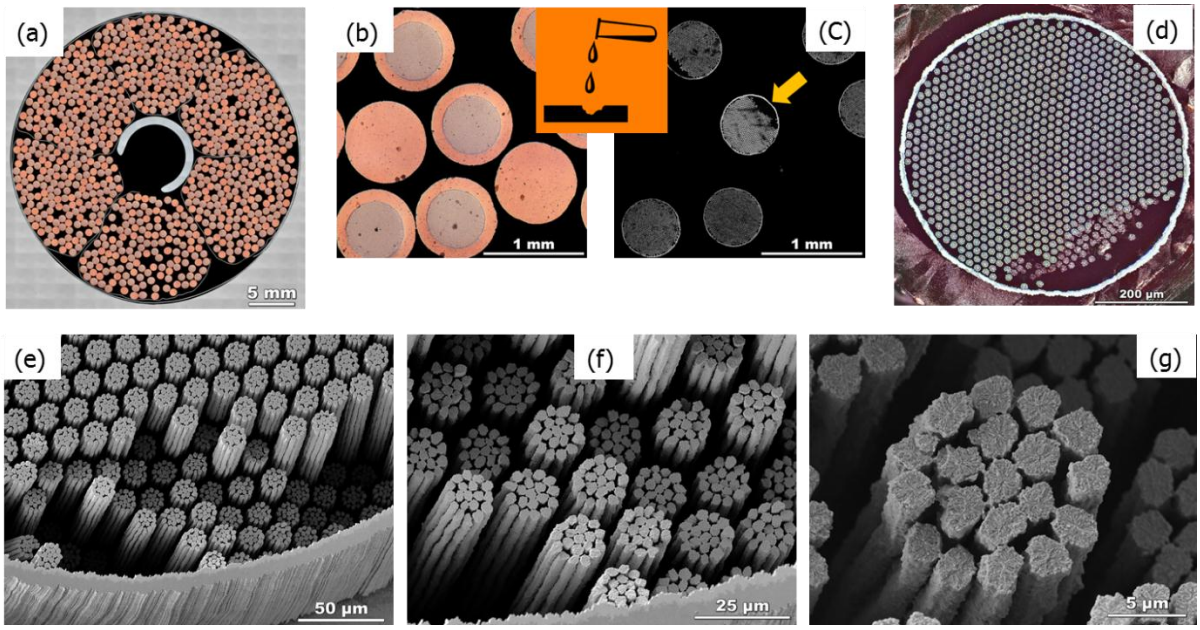

Figure 28: Examples of high resolution images obtained by Florida State University on ITER CICCs: (a) cross section of the High Field Zone of CSJA2, (b) zoom over selected copper and sc strands in cross-section (a), (c) view of sc strands from (b) after copper etching, (e) to (f) FESEM views of broken filaments in multifilament area of etched strand (d) (courtesy of P. Lee and C. Sanabria, Florida State University).

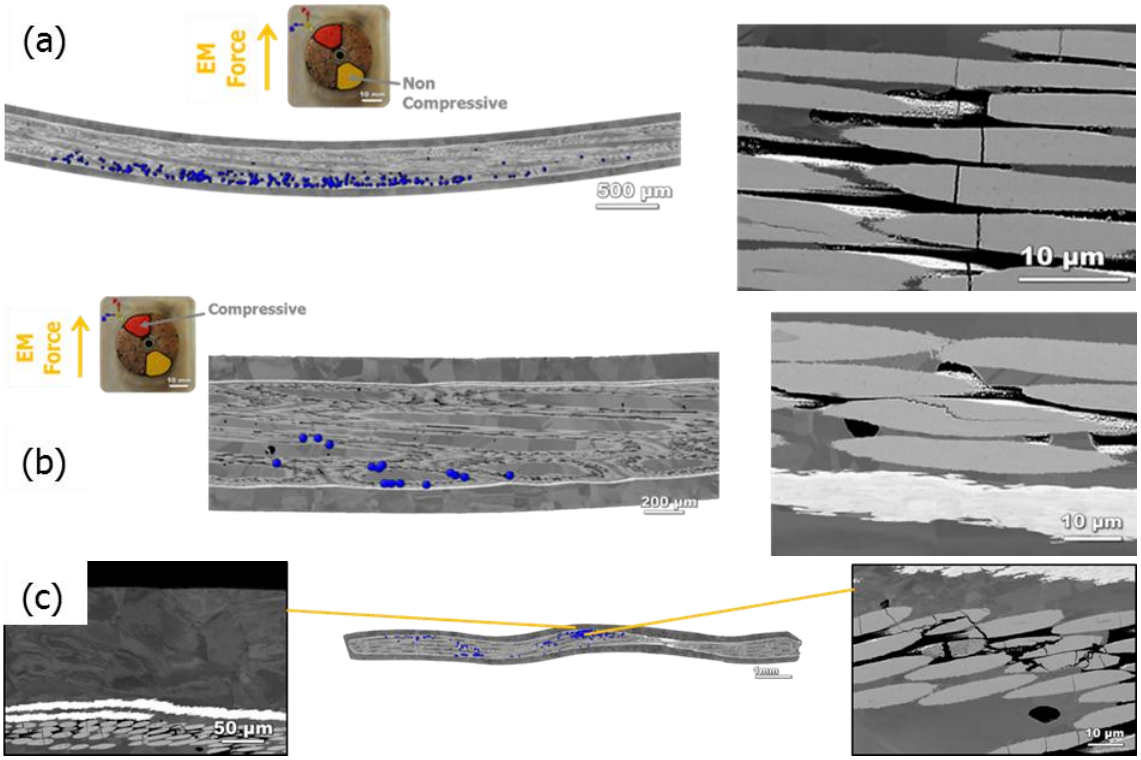

Figure 29: Different crack types observed by LSCM or SEM on ITER-type CICCs: (a) tensile strain cracks (top), (b) contract stress cracks (middle) and (c) mixture of tensile strain and contract stress cracks (bottom; courtesy of C. Sanabria, Florida State University).

ITER-IO contracted FSU to carry out autopsies of the CSIO SULTAN samples. One of the goals of these autopsies is to look for cracks in strands extracted from both the High Field and Low Field sections, and, in the case of the High Field Zone, to compare compressive and non-compressive sides and see if strand buckling/cracking is observed as for the CSJA1 sample. Of course, strand extraction and polishing require a great care to prevent unwanted handling degradations [86].

Cracks are observed using either a Laser Scanning Confocal Microscope (LSCM) or a Scanning Electron Microscope (SEM). In the course of these autopsies, FSU identified different crack categories corresponding to different initiation mechanisms [86]. The first type is tensile strain cracks, which are mainly observed on the tensile side of bent strands extracted from petals on the non-compressive side of the cable, (see Figure 29(a)). Filament fractures run perpendicular to the strand axis and extend over several filaments. The second type is contact stress cracks, which are mainly observed close to copper areas with a finer grain structure than in the rest of the copper in strands extracted from petals on the compressive side of the cable (see Figure 29(b)). Filament fractures run more or less parallel to the strand axis and the finer grain structure is an evidence of cold work. As the copper is expected to be fully annealed during the Nb_3Sn heat treatment (which includes a high temperature plateau at 650 °C for 100 to 200 hours), the cold work can only originate from the compressive strain applied to the strands as a result of the Lorentz forces. The third type is a mixture of the first 2 types, where filament fractures assume different orientations and/or follow zig-zag paths (see Figure 29(c)).

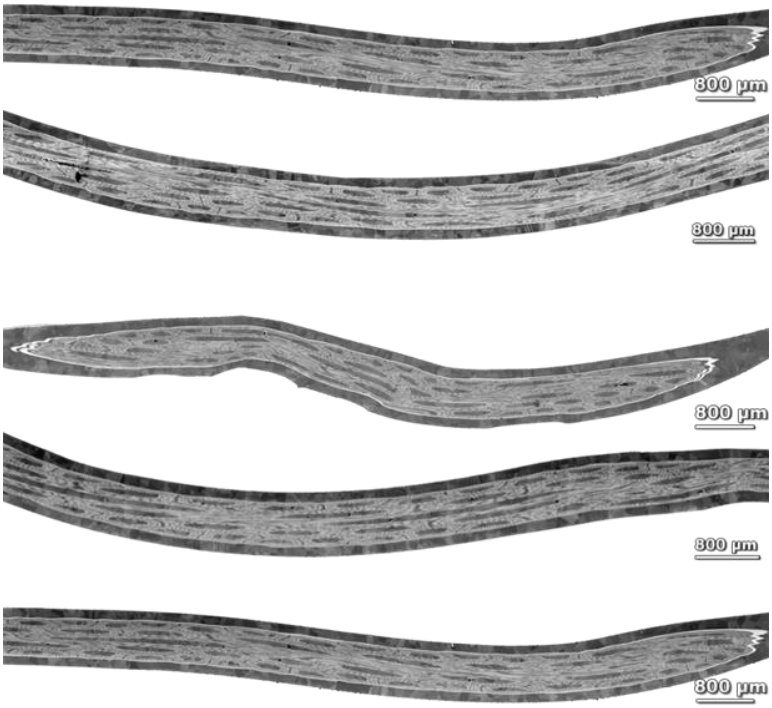

Figure 30: LSCM images of strands extracted from the Short Twist Pitch leg of CSIO2 where no crack was observed (courtesy of C. Sanabria, Florida State University).

In order to gather statistics and to be able to compare the four legs of the CSIO samples a number of strands were randomly extracted from specific areas of selected petals in the cable after jacket removal [86,87]. This comprehensive selection, meant to cover a wide array of strand configurations, includes straight and bent strands located at the corners, medium part and narrow edge of petals coming from the compressive and non-compressive sides of the cable high field and low field zones. A color coding was applied to retain the strand original location. The main results of these crack counts are

- No crack was ever observed in strands extracted from the low field zones, thereby confirming that thermal strains alone are not enough to induce filament fracture,
- Ample evidences of filament fracture was observed in strands extracted from the high field zones of all CSIO sample legs, except for the short twist pitch one where, as illustrated in see Figure 30, none of the inspected strands exhibited any crack.

This clear cut result is quite remarkable and FSU is presently carrying out an autopsy of one of the legs of CSJA3 to assess whether or not short twist pitch conductors relying on bronze strands are also devoid of cracks.

The fact that no filament fracture is observed on the STP leg of CSIO2 is a confirmation that, as predicted by Multifil, the short twist pitch (STP) sequence, where the strands are tightly entangled, offers better strand support against the Lorentz forces during energization, thereby preventing the deleterious displacement and/or bending at the origin of strand degradation.

4.3.8 CS Cabling Degradation

The reliance on short twist pitches and tight compaction has resolved the issue of performance degradation as a function of electromagnetic and thermal cycling, but has given rise to another problem. Destructive examinations (DE) of STP conductors carried out under the supervision of JAEA after cable insertion and compaction have revealed severe strand deformations at the strand crossovers in the cable [88]. As illustrated in Figure 31, it appears that the copper strands (top and bottom left) are more heavily deformed than the superconducting strands (top and bottom right). It also appears that, in the case of internal tin strands (Fig. 31(b), top right), these transverse deformations may result in the collapse of the multifilament area, whereas in the case of bronze strands (Fig. 31(b), bottom right), the multifilament area stay more or less round. Let us note that these deformations are applied prior to heat treatment and brittle Nb_3Sn compound formation.

Deformations to that extent may have never been observed in CICCs but are reminiscent of those observed at the edges of Rutherford-type cables developed for high-field accelerator magnets [89]. In the case of accelerator magnets, it has been shown that with a proper selection of cabling parameters, the I_C degradation due to cabling can be minimized to about 5% [90].

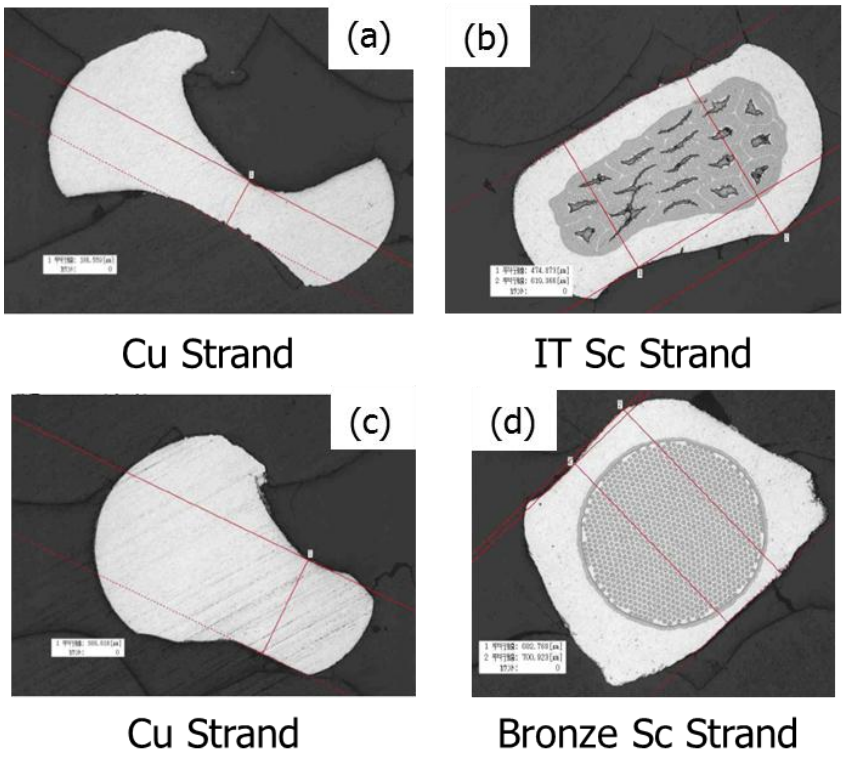

Figure 31: Destructive examinations of short twist pitch conductors showing evidences of strand deformation as a result of cabling: (a) and (b): copper and superconducting strands from a CSIO-type conductor with internal tin strands, (c) and (d) copper and superconducting strands from a CSJA-type conductor with bronze strands (courtesy of Y. Takahashi, JAEA).

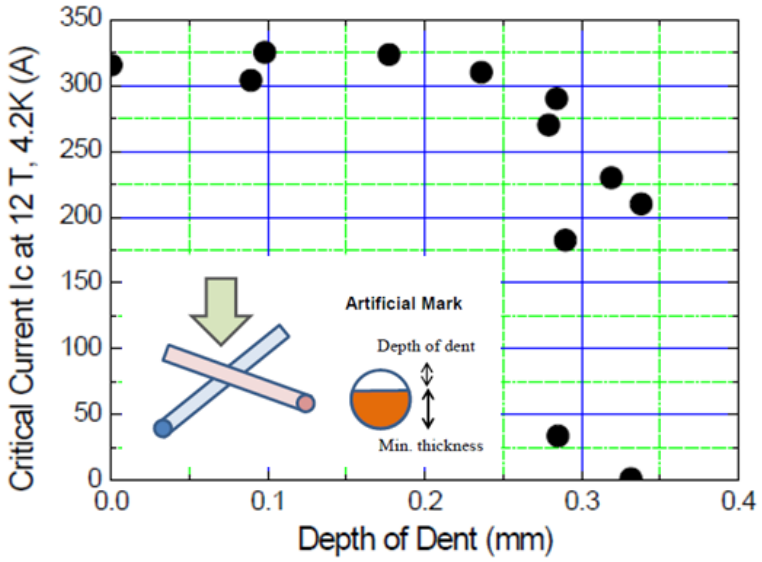

Figure 32: I_C degradation measured on a bronze-type ITER CS strand as a function of depth of indentation simulating strand cross-over in a STP cable (courtesy of Y. Takahashi).

To assess the effects of cabling degradation on ITER-type strands, JAEA has carried out a series of critical current measurements on dented strands [88]. Figure 32 summarizes the results which show that the I_C degradation is negligible for dents below 0.25 mm. This provides a practical criterion on how much cabling deformation is acceptable during production. Potential Japanese suppliers for CS cables have already demonstrated that they were able to produce long lengths of short twist pitch cables where the superconducting strand deformations are maintained below this threshold.

Let us note that after years of divergence between most of the fusion and accelerator magnet communities on how to design Nb_3Sn conductors, there now seems to be an agreement that the most suitable way to prevent degradation is to block Nb_3Sn strand bending/displacement, even at the expense of cabling deformation.

5. Production Status

5.1 TF Conductor Production

5.1.1 Strands

As of today, ~450 tons (95,000 km) of Nb_3Sn strands have been produced; this corresponds to about 95% of the total amount needed for the TF conductors. It is the largest Nb_3Sn strand production ever and has called for a significant worldwide production ramp up. Indeed, the pre-ITER world production was estimated at ~15 t/year. As illustrated in Figure 33, it has been steady for the last four years at ~100 t/year.

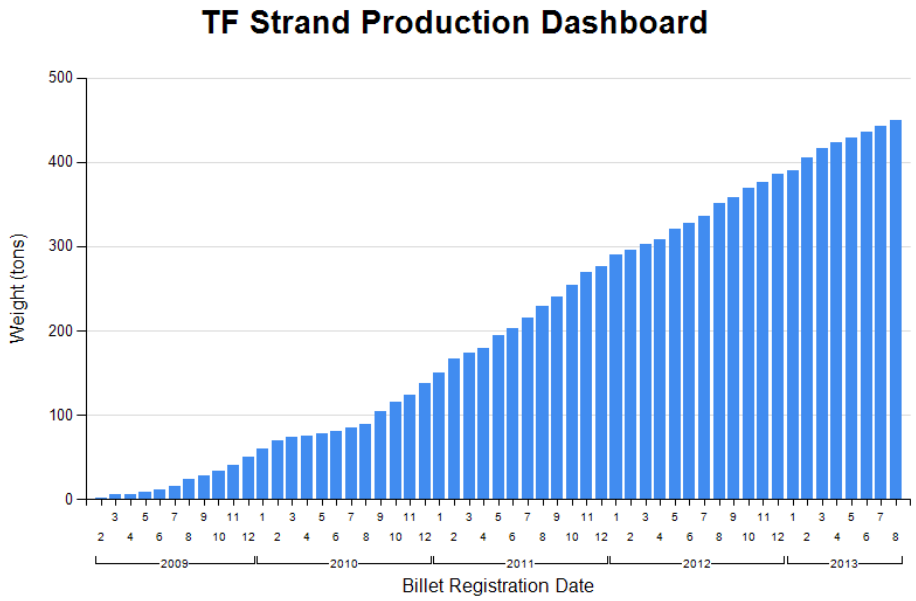

Figure 33: Dashboard of TF strand billet registration into the ITER-IO Conductor Database (in metric tons).

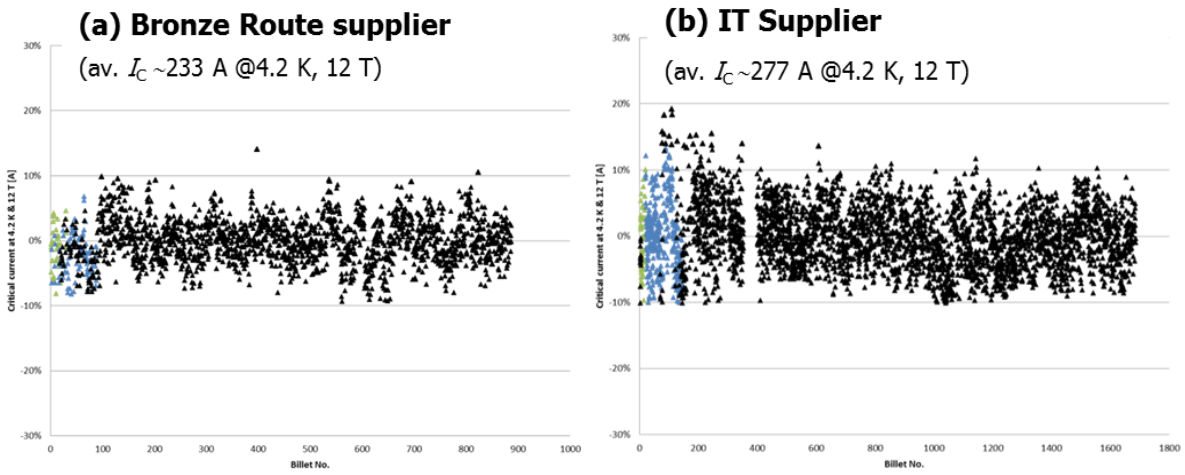

Figure 34: Summary plots of I_C normalized to I_C average (on ITER barrel at 4.2 K and 12 T) versus billet number for the production of 2 ITER TF Nb_3Sn strand suppliers relying on similar billet size (~60 kg): (a) bronze route supplier (left), (b) Internal Tin (IT) route supplier (right) (courtesy of M. Jewell and N. Sullivan, University of Wisconsin at Eau Claire),

Strand suppliers have been required to implement Statistical Process Control (SPC) on critical parameters such as critical current, I_c (4.2 K, 12 T), and hysteresis loss, Q_h (4.2 K, ±3 T). Figure 34 presents typical production data from one bronze and one Internal Tin supplier, both relying on similar billet sizes. It appears that, for the bronze process, the I_c (4.2 K, 12 T) can be kept within ± 10%, while for the IT process, the I_c (4.2 K, 12 T) variations reach ± 15%. Note that these variations cannot be explained by Cu-to-non-Cu ratio variations and, therefore, are likely due to manufacturing tolerances and process variability. The production data also show that Q_h (4.2 K, ±3 T) is more difficult to control for Internal Tin strands than for bronze strands.

The parameter under SPC that proves the most difficult to control for several strand productions turned out to be (rather unexpectedly) the Residual Resistivity Ratio (RRR), which, according to technical requirements should be greater than 100 [15]. Considerable efforts were deployed in order to address this problem. At least 3 factors have been identified as having an influence on the RRR, in particular in the case of wires for which the high temperature plateau during heat treatment exceeds 100 hours

- cleanness and quality of strand surface during production so as to prevent entrapment of impurities underneath the chromium layer that may diffuse during heat treatment and pollute the strand copper,
- cleanness of the heat treatment furnace (in particular, for vacuum furnace) and choice and purity of the inert gas in the case of furnaces with inert gas atmosphere. In particular, in the case of furnace with inert gas atmosphere, it is critical to control the presence of O_2 that can have deleterious effects on the results leading to significant overestimation [91],

- stability and reproducibility of the sample temperature for the measurements near 20K. In particular, the sample holder must be designed to avoid temperature gradient and must be equipped with accurate temperature sensors that properly assess the sample temperature.

As a result of these investigations, the heat treatment of 3 of the suppliers, which called for a 200 hour high temperature plateau, had to be modified. For two suppliers, the plateau was reduced to 100 hours [92], whereas for the 3rd supplier, the plateau temperature was reduced.

Another issue is the type of Cr used for electroplating. Seven suppliers chose hexavalent chromium, Cr^{+6}, which is widely used in the industry because of its hardness and durability, while one supplier chose trivalent chromium, Cr^{+3}, which poses less health and safety issues and is generally used for decorative purposes. Although there were concerns from the start [93], the latter supplier managed to develop a stable Cr^{+3} plating process, which passed all acceptance tests on strands, including flaking test (after winding on a 3-diameter rod). However, a serious peeling problem occurred during the first cabling trials of Cr^{+3} coated strands, where millimeter long chips of Cr/Cu appeared to accumulate at the forming die during 1st and 2nd stage cabling, resulting in a galling-life effect that further enhanced the peeling (see Figure 35(a)). Such peeling was not observed during the cabling of Cr^{+6} coated strands on the same equipment with the same setting (see Figure 35(b)). A comprehensive program was carried out to study the effect of die size, die material, and strand angle at die entrance and a practical solution was eventually found where very little to no dust is observed at the die and minimal scrapes or damages are observed on the cabled strands. This solution will be implemented for the cabling of the trivalent chromium plated strands (which has yet to be done). This problem, which hopefully has been overcome, is a reminder that it is not advisable to deviate from validated processes as it may have un-anticipated consequences on subsequent manufacturing steps which can be difficult to recover.

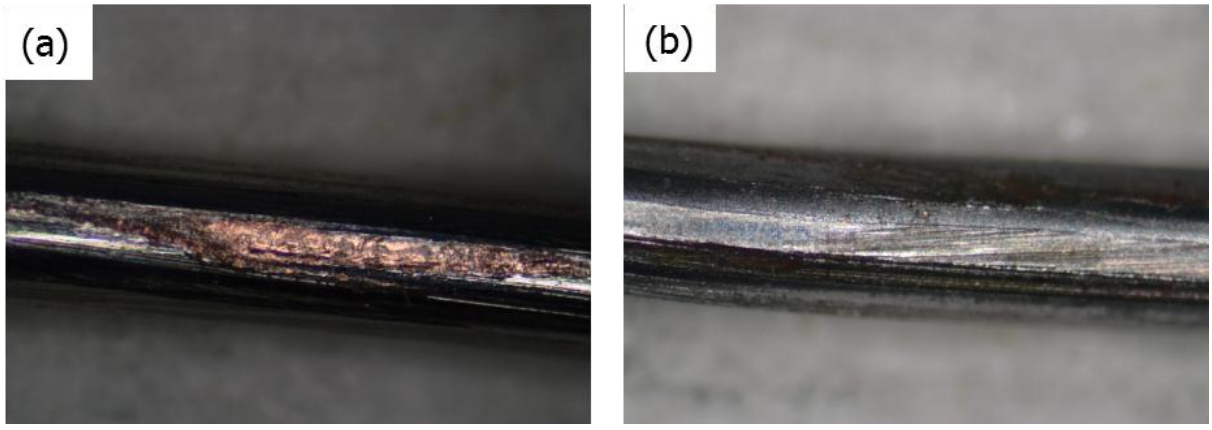

Figure 35: examples of damages observed on the surface of Cr-plated IT Nb_3Sn strands as a result of cabling: (a) Cr^{+3} plated strand showing evidence of Cr/Cu peeling and (b) Cr^{+6} plated strand (courtesy of M. Jewell and J. Luhmann, University of Wisconsin at Eau Claire).

In spite of these difficulties, and although there are some differences among suppliers, the 8 TF strand productions, which have been completed or are very near completion, can all be considered as successful, in particular, those of the 3 new suppliers who started operation for the purpose of ITER. Instrumental to this success were the systematic low temperature measurements that were required from the suppliers and the verification measurements carried out by independent parties, whose sampling rate was modulated, depending on the production phases and the quality of the production and of the supplier data. The verification measurements led to the identification of issues that otherwise would have gone unnoticed, all the more that these were the first large scale productions of Nb_3Sn strands for which much less experience was available than for Nb–Ti strands. Also critical was the organization by ITER-IO of several rounds of benchmarking of Nb_3Sn (and also Nb–Ti) strand test facilities of all interested parties (suppliers, DA and ITER-IO reference laboratories) to ensure consistency of the measurements and of the corresponding acceptance criteria [29,94]. Note that for strand benchmarking, ITER-IO selected CERN as its reference laboratory [95-96]. As part of its scope of work, CERN was asked to derive a $J_C(B,T,\varepsilon)$ parameterization for ITER Nb_3Sn strands that is now used by all ITER partners [95].

In summary, the ITER project has enabled Nb_3Sn strand production to achieve a maturity similar to that of Nb–Ti strand production and, hopefully, a higher cost efficiency that should spin off new markets.

5.1.2 Jacket sections

The jacket sections for the TF conductors are made up of modified 316LN [15]. The mother heats are required to be subjected to an Electroslag Remelting (ESR) to limit the risk of macro-inclusions. The jacket sections are produced by hot extrusion followed by cold drawing and/or pilgering steps with some intermediate and a final solution annealing step. The final products are white pickled or bright annealed. Every jacket section is inspected by NDE techniques. Product analyses and detailed tests are also required on every jacket section lot, to check, among others, the grain size, ferrite content, and whether there are micro-inclusions and inter-granular corrosions. In particular, it is required to verify on the final product that the material is located in the austenite region above the 0% ferrite line in the Delong phase diagram [97] and that no ferrite traces are visible on micrographs at a magnification of 500x.

In addition, the PA defines requirements on the mechanical properties of the jacket sections at cryogenic temperatures. The measurements are carried out on samples of standardized geometry that have been prepared to be representative of the material state during coil operation, including the cold work that is generated during compaction, spooling, straightening and winding, and the ageing due to Nb_3Sn heat treatment. For TF, the samples must be cut by electrical discharge machining or water jet from a jacket section which has been compacted to final conductor dimension, stretched 2.5% at room temperature and heat treated at 650 °C for 200 hours in an atmosphere of inert gas or vacuum [98].

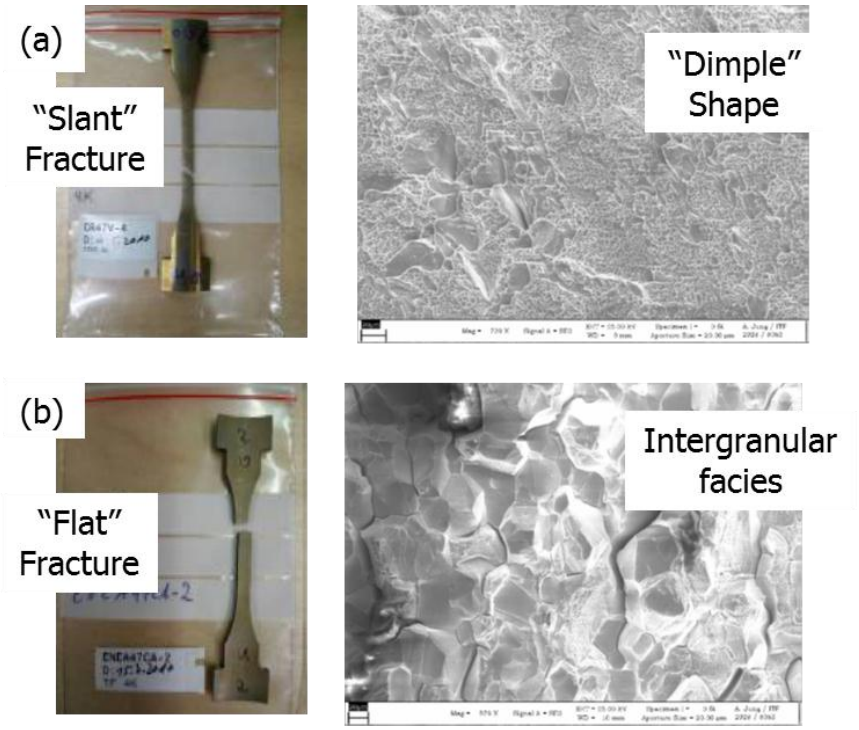

Figure 36: examples of fracture features of tensile test specimen cut from ITER TF tubes (after compaction, stretching and ageing): (a) sample with fully ductile fracture and maximum elongation above 20% and (b) sample exhibiting embrittlement and maximum elongation lower than 15% (courtesy of K.P. Weiss, KIT).

For TF jacket sections, the temperature/duration of the Nb_3Sn heat treatment are sufficient to produce some limited grain boundary sensitization. The latter, combined with the effect of cold work produced during compaction and subsequent handling operations, can induce a loss of ductility at 4.2 K. Hence, it is critical to characterize the resulting level of embrittlement and to ensure that the material behavior is predominantly ductile in the stress range of interest. As the TF tube thickness (~ 2 mm) is too small to enable the preparation of suitable samples for fracture toughness (K_{IC}) and fracture crack growth rate (FCGR) measurements, it was decided to circumvent this difficulty by implementing a specification on the maximum elongation of at least 20% below 7 K. It is also required to carry out a micrographic examination of the fracture surfaces so as to assess the extent of the dimple pattern zone, resulting from ductile fracture, and of the inter-granular surfaces, resulting from brittle fracture caused by grain boundary sensitization [99]. This is illustrated in Figure 36 which shows examples of tensile test specimens cut out from TF jacket sections after compaction, stretching and ageing. Figure 36(a) illustrates a successful specimen, which features a shear fracture at a slant of approximately 45° and for which the broken surfaces exhibit a clear dimple shape that is consistent with a ductile fracture. The maximum elongation of this sample was above 20% and met PA requirements. Figure 36(b) illustrates an unsuccessful specimen, which broke with a flat fracture and for which the broken surfaces exhibit a clear pattern of intergranular fracture that reveals embrittlement. The maximum elongation of this sample was below 15% and did not meet PA requirements.

The qualification of TF jacket suppliers turned out to be a bigger challenge than anticipated, in particular due to the requirements on maximum elongation after compaction, stretching and ageing. At first, only 3 companies in the world were qualified: KSST in Japan [100,101], POSCOSS in Korea [20,102] and Jiuli in China [16,103]. A European supplier, SMST, is now in the process of being qualified. The parameters influencing the maximum elongation have not yet been clearly identified, therefore, as for the superconducting strands, once a supplier has been qualified, the PA calls for a tight control of chemical composition and manufacturing processes. During production, maximum elongation measurements must be carried out on samples from every cast heat. Figure 37 presents a summary plot of these measurements for all the heats that have been used up to date across all 6 DAs. The data appear to meet the 20% specification. As for the strands, IO has organized a benchmarking of the various mechanical test facilities used by the DAs with KIT in Germany acting as the ITER-IO reference laboratory [98]. The data of Figure 37 show a reasonable agreement between KIT and DA measurements. The ITER-IO also funded a contract with the Kurchatov Institute in Moscow, Russia to compare the results of mechanical tests on sub-size samples and full-size jackets, but more work would be needed to assess the reliability of the measurements on full-size jackets [104].

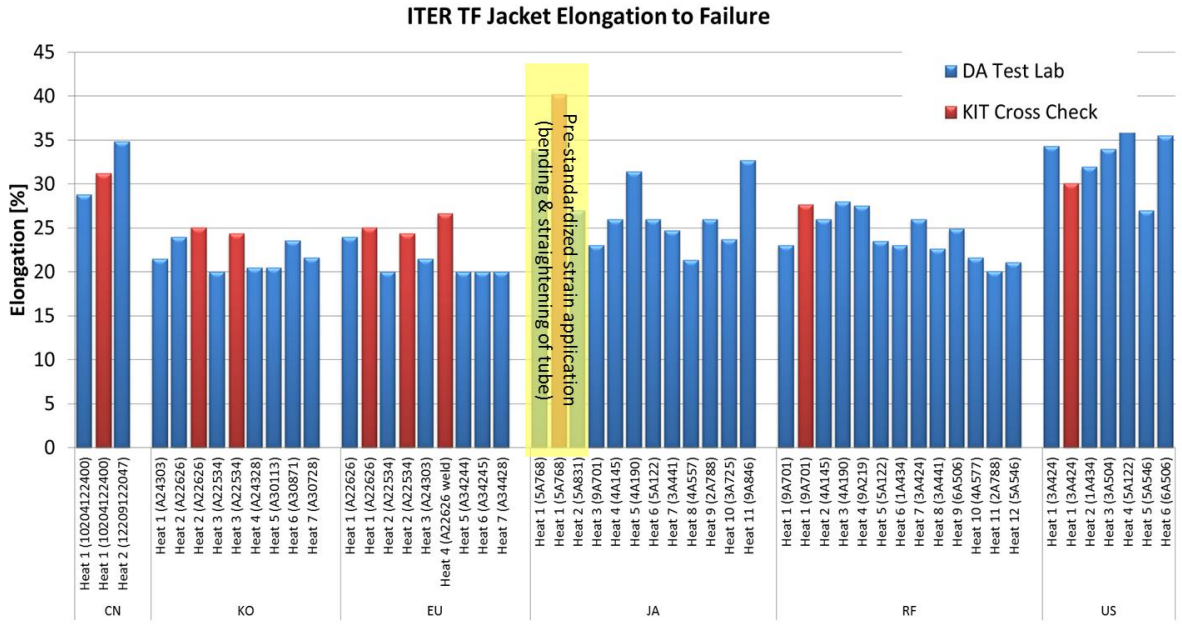

Figure 37: Summary plot of maximum elongation measured on tensile specimens issued from TF jacket samples at cryogenic temperature for the productions of all six DAs. The blue bars correspond to data from DA reference laboratory, while the red bars correspond to data from ITER-IO reference laboratory.

This manuscript was submitted to Superconductor Science & Technology (IOP) for possible publication
This manuscript was published by Superconductor Science & Technology (SuST, IOP) 27, No. 4, 044001, (2014).

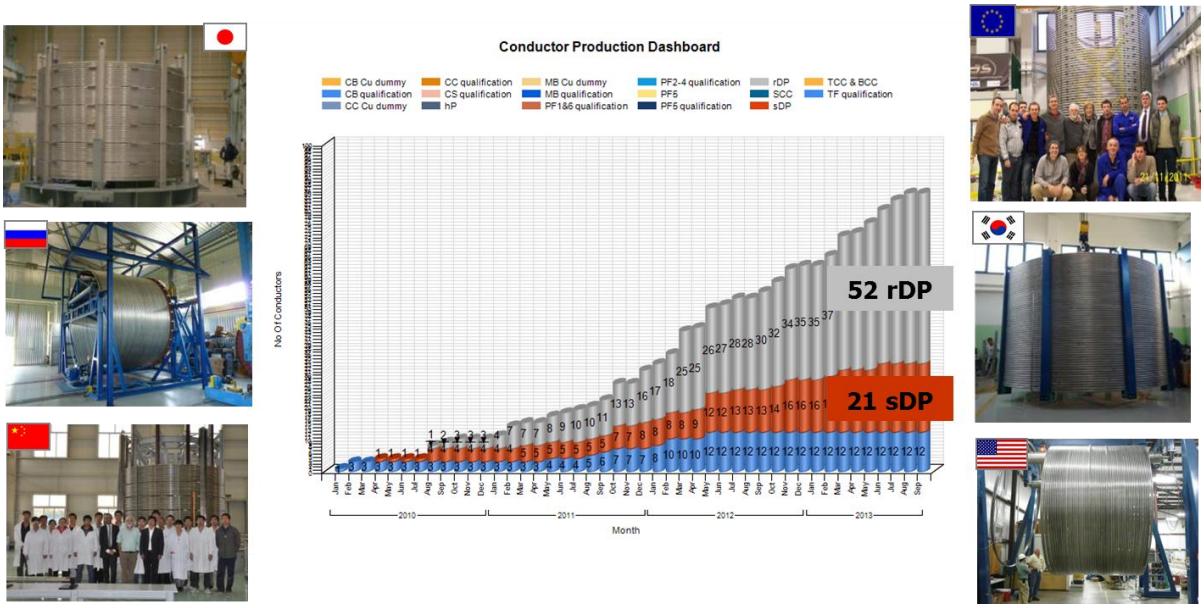

Figure 38: Dashboard of TF conductor registration into the ITER-IO Conductor Database, including 760 m long regular double pancake (rDP) and 415 m long side double pancake (sDP) unit lengths.

5.1.3 Conductors

In addition to 12 copper and superconducting qualification unit lengths, a total of 52 x 760 m regular Double Pancake unit lengths and of 21 x 415 m side Double Pancake unit lengths have been manufactured by JA, KO, RF, EU and CN (see Figure 38). This corresponds to ~10 Toroidal Field Coils and more than half of the conductor unit lengths required for the TF coils.

Two unexpected issues were encountered in the early stages of PA execution

1) According to the conductor PA requirements, the orbital welding of the jacket sections must be carried out in accordance with the rules of ASME Sections VIII and IX. This calls for welder certification and third party inspection of the welding process qualification.
2) According to EU regulations, for the conductor spools to be delivered to the EU, the lifting fixtures of the transportation jigs must be CE marked.

This caused long delays (up to one year) for the 2 DAs (CN and RF) who were lacking experience with these procedures.

As of today, three major incidents have been recorded at 2 suppliers during jacketing operations. At one supplier, the steel leader rope that is used to pull the superconducting cable inside the jacket assembly broke in the area of the grip between leader rope and sc cable after 680 m (out of 760 m) had been inserted. A cumbersome but clever rescue plan was developed. To avoid damaging the cable by de-inserting it from the tail end in the opposite direction to insertion (see Figure 11), the whole jacket assembly was pulled from the tail end; the friction forces thus generated between cable and jacket were in the same

direction as during insertion. The operation was successful and after thorough inspection of the cable surface and outer dimension, it was agreed that the cable could be reused for a subsequent insertion. The other 2 incidents occurred at another supplier and were more dramatic. In one case, a cleaning rug was left on the conductor jacket as it entered the compaction machine. This rug produced a large dent on the conductor surface. Fortunately, this conductor Unit Length was 760 m long (to be used for the winding of a so-called regular double pancake or rDP) and the dent location enabled the supplier to salvage 415 m of good conductor (that could be used for the winding of a so-called side double pancake or sDP). Hence, this rDP UL was converted into an sDP UL. In another case, a sudden increase of pulling force was observed during the insertion of an rDP cable into a jacket assembly after about 40 m had been inserted. The decision was taken to stop insertion and to de-insert the cable by pulling it in opposite direction. The reason for this blockage was found to be a local waviness in the cable (whose diameter was otherwise within specifications). Attempts were made to correct this waviness (by re-taping the stainless steel outer wrap), but they were unsuccessful and the cable UL had to be discarded. It should be noted that PA specification calls for the use of a go-no-go gauge of length 60 cm, oversized by 0.1 mm on the maximum allowable cable diameter to be applied prior to cable spooling so as to check for this kind of waviness, but the cabling company and the DA objected to the use of such go-no-go gauge and filed a deviation request, which, after long discussions, was eventually agreed by the ITER-IO. This is a reminder that technical requirements that have been developed over many years based on practical experience should not be neglected or tampered with.

Another recurrent issue has been that of cleanliness of conductor spools. Having full jacket assemblies laying for days or even weeks in the jacketing lines can result in an accumulation of dust, insects and even droppings on the conductor surface. All conductor suppliers have now implemented several cleaning stations, usually before and after the compaction machine, to clean the conductor jacket. In addition, all delivery packages include sealing bags and a large amount of desiccant to protect the conductor spools during transportation and storage.

5.1.4 Conductor delivery and storage

ITER-IO acknowledged very early that conductor delivery packages were a critical interface between conductor supplier and coil manufacturer and organized, starting in August 2008, a series of meetings involving the 6 conductor DAs, the 2 TF coil DAs and their suppliers to discuss conductor spooling and transportation. It was decided that each of the conductor DAs would generate a standard set of documents, including a design report for the transportation jig and package (including stress analysis), 2D drawings, and an unpacking procedure to be reviewed by the relevant TF coil DA and approved by ITER-IO. The discussions went on until the spring of 2012, when the first delivery packages from CN, KO and RF were finally agreed with JAEA and Fusion For Energy (F4E, acronym for the European Domestic Agency). One of the reasons why it took so long is that, at this time, the conductor DAs were well ahead of the TF coil DAs, whose contracts with TF coil suppliers were barely in place.

The ITER-IO efforts on defining and standardizing conductor delivery packages, successful for the conductors delivered to JA, did not prevent an interface issue from arising at the time of the first RF conductor deliveries to F4E. The unspooler installed at the F4E TF coil supplier could only handle a cylindricity tolerance on the conductor spool of +/- 3 mm, much tighter than the alignment specified to the conductor suppliers, who, for some of them, can only achieve down to +/-6mm. The unspooler jammed in early trials. Review by an independent tooling expert confirmed the need to modify the unspooler and offered options to cope with this problem at a minimum cost [105]. This issue, which is quite trivial from the technical point of view and which, in a normal project environment would have been easily resolved by upgrading or replacing the unspooler, became the object of a contentious dispute over responsibility and cost, which led to blocking of deliveries of RF conductor spools and forced RF to interrupt its jacketing operation for several months. This issue provides a good example of the management challenges offered by ITER, which are far more difficult to address than the technical problems in an organization where no clear lines of authority have been defined.

Outside of this issue, deliveries of TF conductor ULs to TF coil suppliers are now taking place on a regular basis but they still remain a logistics challenge. This is particularly true for CN, who is required to deliver TF conductor ULs to both F4E and JA, and for KO, whose cables and jacket sections are manufactured in KO before being shipped to EU for jacketing, then jacketed conductor spools are shipped back from EU to KO before final delivery to JA.

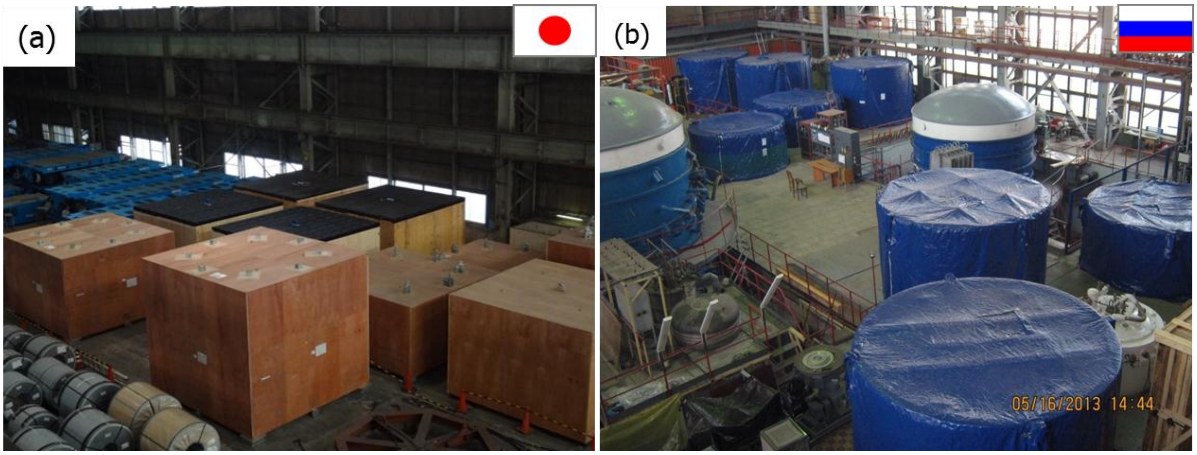

Figure 39: Storage of TF conductor ULs: (a) CN, KO and TF ULs in a warehouse rented by JAEA in Wakamatsu, Japan (left, courtesy of Y. Nunoya, JAEA), (b) RF ULs at the Kurchatov Institute in Moscow, Russia, awaiting F4E's agreement to ship to EU (right, courtesy of V. Tronza, RF-DA).

In overall, TF conductors, for which all industrial contracts have been placed and are running at full speed, are produced at a faster pace than they can be used for winding. The need for storage space was identified very early by JAEA who has been renting a warehouse in Wakamatsu (near the NSSE jacketing line) since May 2010. This warehouse, depicted in Figure 39(a), is used to store conductor unit lengths delivered from CN, JA and KO and destined to coil winding in Japan. F4E is far more reluctant to cover storage costs for conductor spools delivered well ahead of their actual need dates. Figure 39(b) shows the RF conductor unit lengths which are kept at the Kurchatov Institute in Moscow awaiting resolution of the aforementioned conductor spool misalignment dispute.

5.2 CS conductor production

5.2.1 Strands

As already mentioned, JAEA has placed contracts for the manufacture of the conductors (one 613 m quadripancake or qP and six 918 m hexapancake or hP ULs) for the bottom module of the CS coil stack (CS3L). Calls for tender for the other modules are underway.

The CS3L strand/cabling contract was awarded to Jastec (in consortium with Mitsubishi Cable), who has developed a new generation of Nb_3Sn bronze strands with I_C in excess of 260 A, comparable and even higher than that of IT Nb_3Sn strands for ITER [70]. As illustrated in Figure 40, more than 14 tons of CS strands have already been registered into the ITER conductor database. As discussed in section 4.3.8, there were some initial issues with cabling degradation, but the process is now under control.

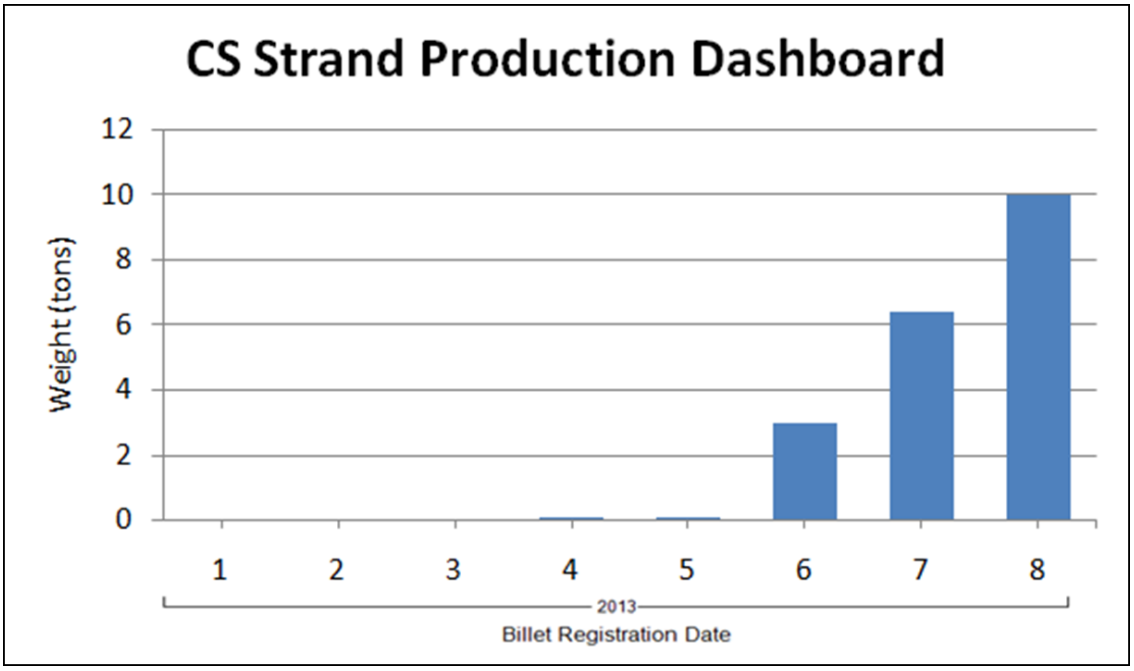

Figure 40: Dashboard of CS Nb_3Sn strand billet registration into the ITER-IO Conductor Database: (in metric tons).

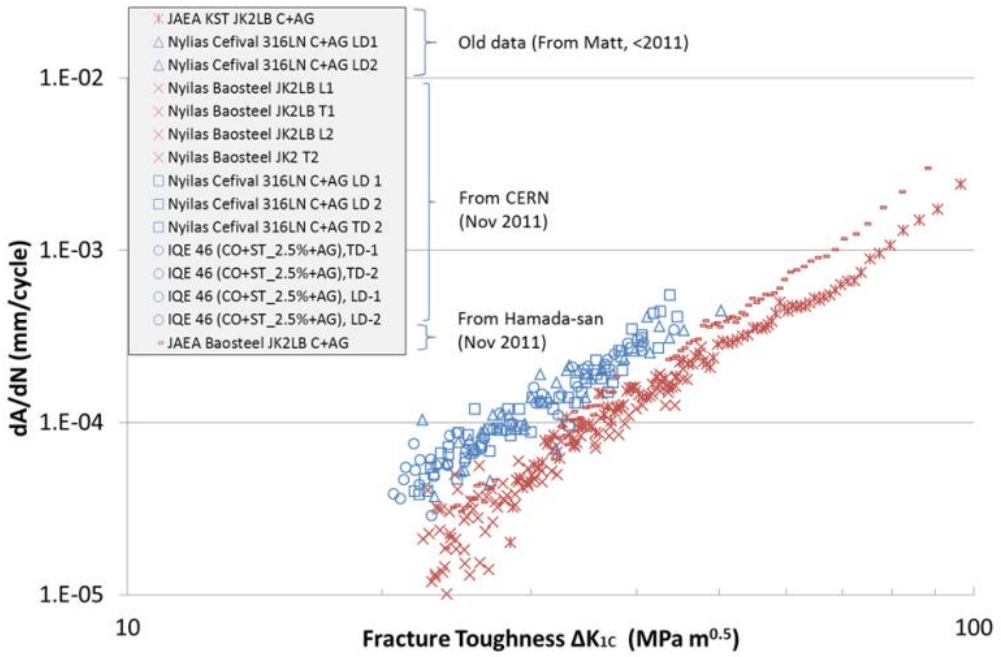

Figure 41: Summary plot of FCGR measurements on specimens cut from compacted and aged 316LN and JK2LB jacket sections produced for ITER CS (Courtesy of I. Pong, LBNL).

5.2.1 Jacket material

The CS conductors rely on a circle-in-square jacket. In the 2000s, JAEA developed with Kobe Steel, LTD, a special grade of austenitic steel with high manganese and low carbon contents and boron addition, referred to as JK2LB. JK2LB has a lower integrated thermal shrinkage coefficient between room temperature and 4.2 K than that of conventional 316LN [106-107]. Utilizing the thermal shrinkage differential between the conductor jacket, made up of JK2LB, and the so-called tie plates, made up of NITRONIC® 50 (XM-19), featuring an integral thermal contraction between room temperature and 4.2 K similar to the one of 316LN [108], enables the application of a suitable axial pre-compression to the CS coil stack at the end of cooldown without overstressing the tie plates at room temperature [109]. However, in 2008-2009, at the time of the CS conductor PA signature, there were concerns that the production costs of JK2LB might be prohibitive. Therefore, ITER-IO decided to revisit the issue of modified 316LN vs. JK2LB and launched an R&D program with Baosteel in China and Céfival in France to compare manufacturing costs and mechanical properties at cryogenics temperature [110]. The low temperature mechanical measurements included Fatigue Crack Growth Rate (FCGR) on standardized specimens cut from compacted and aged jacket sections. Figure 41 presents a compilation of available and relevant FCGR data for both 316LN and JK2LB jacket sections [111-114]. The data of Figure 41 clearly show that JK2LB has a slower FCGR than modified 316LN and confirm that it is a more suitable candidate for CS jacket material. A side benefit of the ITER-IO program is that it also helped demonstrate that the production costs of JK2LB were not significantly higher than those of 316LN and the decision was made by ITER-IO in December 2011 to select JK2LB for the CS jacket. The manufacture of the CS conductors will require about 500 tons of JK2LB jackets.

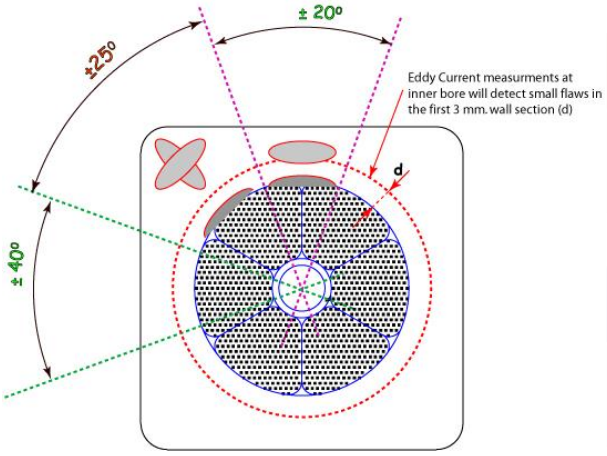

Table 2(a): Max Defect Area, Thin-Wall Region ±20°

Module (Pancake)	Surface or Sub-Surface (d<3) [mm²]	Embedded (d>3 mm) [mm²]
CS1/CS2/CS3U	2	5
CS3L (P7-P40)	7	12
CS3L (P1-P6)	17	20

Table 2(b): Max Defect Area, Corner Region ±25°

Module (Pancake)	Surface or Sub-Surface (d<3) [mm²]	Embedded (d>3 mm) [mm²]
CS1/CS2/CS3U	3	7
CS3L (P7-P40)	10	16
CS3L (P1-P6)	20	30

Figure 42 and Table 2: Maximum allowable defect sizes computed by LEFM for the conductor jackets in the various CS modules as a function of defect location. "d" represents the depth to the edge of the flaw with respect to either the cable-side or jacket outer surface; any surface flaw has d=0. Pancakes in CS3L are numbered from the bottom of the module. (courtesy of C. Jong, ITER-IO, and K. Freudenberg, L. Myatt, K. Cochran, US-IPO).

5.2.3 Maximum flaw sizes and jacket NDE

As for the superconducting strands, the CS jacket sections and welds will have to sustain a large number of stress cycles. A very thorny issue has been the assessment of the maximum allowable defect sizes. This assessment is carried out by relying on Linear Elastic Fracture Mechanics (LEFM) analyses. It requires distinguishing between sub-surface and embedded defects and it depends on the defect location (thin wall or corner area of the circle-in-square jacket). In the assessment, the effect of important assumptions about the stress state, like residual stresses and mean stress corrections (Walker coefficient), have been investigated and determined [115-117]. Figure 42 and Table 2 summarize the maximum allowable defect sizes computed by LEFM analyses as a function of defect position in the jacket section for the different modules of the CS coil stack [118]. Defects are assumed to be planar (no volume) and are perpendicular to the hoop stress (winding direction). The data reported here include a safety factor of 2 on the number of cycles and on the defect size and a safety factor of 1.5 on K_{IC}.

Of course, the CS jackets and CS welds must be subjected to a Non Destructive Examination (NDE) which, ideally, should have a good enough resolution to detect defects of the size listed in Table 2. This is relatively easy for the welds, where conventional X-ray methods are good enough to achieve the required resolution, but it is far more difficult for the base material, in particular, in the corner areas. At present, the NDE inspection of the CS jacket sections includes a combination of Phase Array Ultrasonic Testing (PAUT) for the material bulk [111,119] and of Eddy current Testing (ET) for the first 2 to 3 mm from the inner bore of the jacket section. The PAUT inspection is well suited for the detection of the most critical defects which are expected to arise from internal longitudinal stresses provoking delamination [120], with a main component parallel to the maximum flow of the material, *i.e.*, in the extrusion and drawing direction. Delaminations are the bulk defects most expected

in pipes of relatively large cross sectional area and thickness. From the experience developed from the CS circle in square jacket productions to date, the most relevant extrusion defects have been generally identified in the bulk of the pipes with a main component parallel to the extrusion direction [121]. The ET inspection is well suited for the detection of surface defects in the extrusion process which may arise from different origins, such as improper surface quality of the billet, imperfect lubrication and excessive extrusion temperature and/or extrusion speed. However, the combined PAUT/ET inspection does not provide a full proof inspection against embedded transverse defects in the corner areas, but the likelihood of such defects in high purity austenitic steel having been subjected to an ESR is deemed to be very small as such flaws are more likely to develop from the interaction with the die on the surface of the material. Moreover, they are generally not single and isolated but occur in a portion of the extrusion where critical conditions have been met: hence, the probability that they are detected is higher than for a single isolated defect. The optimization of the NDE procedures was quite cumbersome and was carried out with the support of CERN and ISQ in Portugal.

5.2.4 Corrosion effects

It should be noted that JK2LB has one disadvantage: due to its low Cr, Ni and Mo content, it has limited alloying elements conferring corrosion resistance. As a result, exposures to halogen elements (such as HCl for Cr plating removal or ZnCl based soldering flux) should be prevented at all time during conductor/coil manufacture. This sensitivity to corrosion was demonstrated by the first 2 CS conductor samples (CSJA1, prepared in Japan, and CSJA2 prepared at CRPP), which rely on conductors with JK2LB jacket, and which developed a leak during cold testing. In both cases, the leak happened 6 months to one year after sample manufacture, in an area of stress concentration in the JK2LB material which is likely to have been exposed to halogen fumes prior to Nb_3Sn heat treatment. As illustrated in Figure 43, the combination of high stress, corrosive contamination and high temperature heat treatment is believed to have resulted in the initiation of a crack that slowly propagated by stress corrosion cracking along the grain boundaries of JK2LB and, after many months, resulted in a He leak. After these two incidents, great care was taken during all subsequent sample preparations at CRPP to avoid any kind of corrosion and none of the subsequent samples developed a leak. This critical issue should be kept in mind during the manufacture of the CS coil modules at the supplier and the on-site assembly and installation of the CS coil stack in the tokamak.

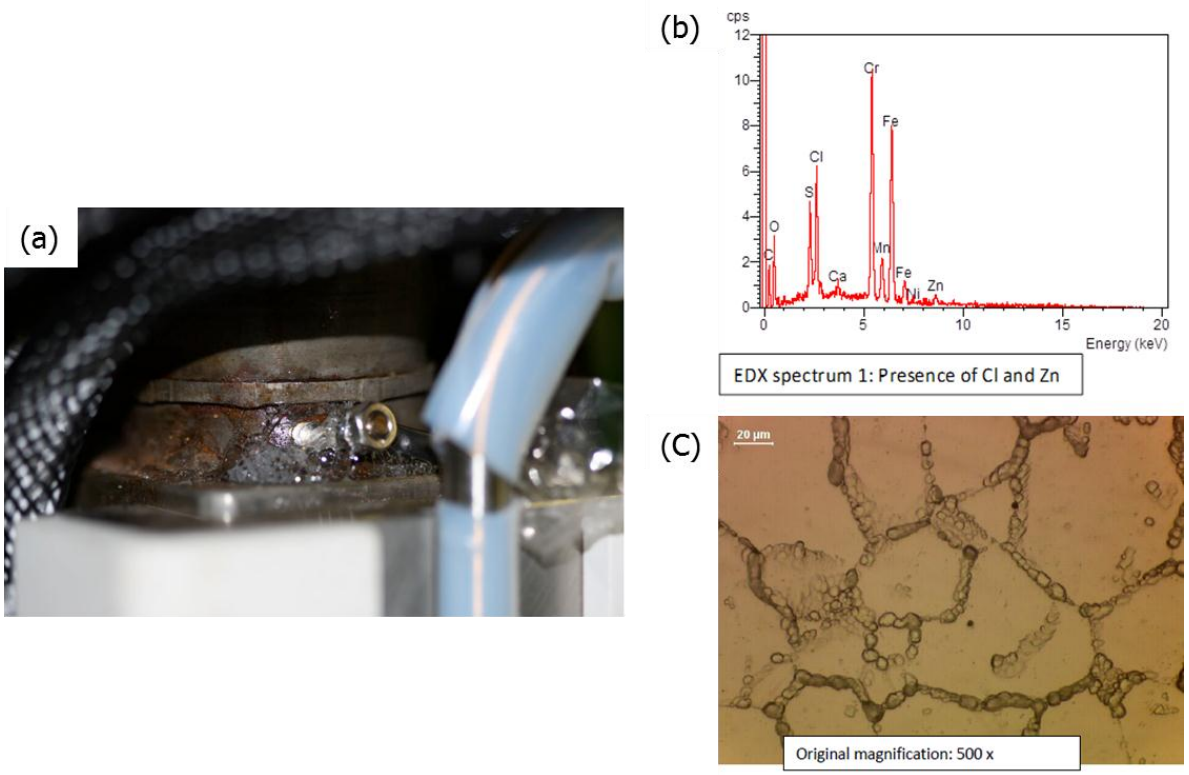

Figure 43: (a) evidence of He leak near the crimping rings of one leg of CSJA2 (left, courtesy of P. Bruzzone, CRPP), (b) evidence of Cl and Zn contamination in the rust residues removed from the leaking area of the test sample. Moreover, microstructural observations confirmed that the material of the conduit is in a slightly sensitized state, with evidence of ditch structure (c) revealed by the oxalic acid etch test (courtesy of S. Sgobba, CERN).

5.2.5 Conductors

NSSE has presently completed the manufacture of the process qualification unit lengths and is getting ready for the welding of the jacket assembly for the first ~600 m quadri-pancake unit length.

5.3 PF Conductor production

Nb–Ti strand types 1 and 2 have been qualified for use in PF conductors through the successful testing of SULTAN samples [122,123]. For these samples, which were prepared by a consortium made up of ENEA Frascati, in Italy, and CEA Cadarache, in France, the bottom joint was replaced by a hairpin to limit the risk of non-uniform current distributions that may arise from the joint [124], and that were believed to be at the origin of the premature quenching observed on previous high current, Nb–Ti SULTAN samples [125].

As illustrated in Figure 44(a), RF and F4E have registered ~95 t of Nb–Ti strand type 1 (out of the required 110 t) into the Conductor Database. RF is in full cable production and F4E is in the process qualification phase for PF1 and PF6 conductor jacketing.

This manuscript was submitted to Superconductor Science & Technology (IOP) for possible publication
This manuscript was published by Superconductor Science & Technology (SuST, IOP) 27, No. 4, 044001, (2014).

In the meantime and as illustrated in Figure 44(b), CN has registered nearly ~78 t of Nb–Ti strand type 2 into the Conductor Database, including 55 t out of the required 155 t for PF2-5. In addition, CN has completed the manufacture of all process qualification unit lengths and is proceeding with the production of PF5 and PF2-4 conductors. Figure 45 shows pictures of the 740 m PF5 copper dummy UL and of the 910 m PF2-4 Cu dummy UL. The PF5 copper dummy was delivered (in 3 sections) to the ITER site on 3 June 2013; this was the very first delivery of a component to ITER.

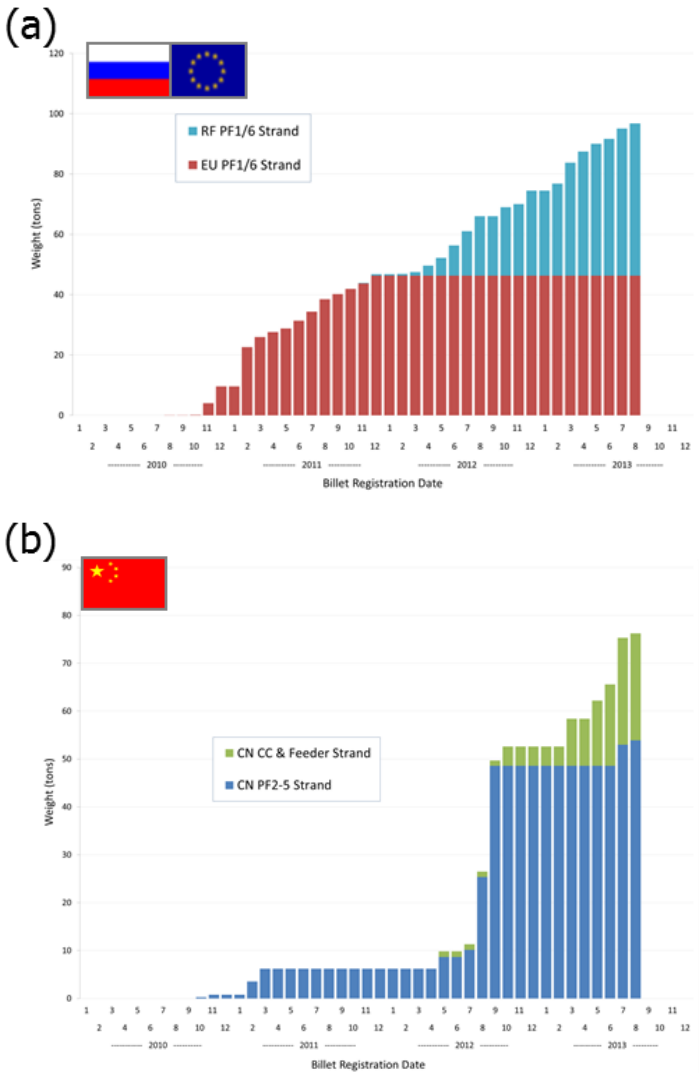

Figure 44: Dashboard of Nb–Ti strand billet registration into the ITER-IO Conductor Database: (a) strand type 1 for PF1 and 6, (b) strand type 2 for PF2-5, CC, MB and CB (in metric tons).

Figure 45: views of first PF conductor ULs manufactured in China: (a) 740 m long Cu dummy UL and (b) 910 m long Cu dummy UL (Courtesy of Y. Wu, ASIPP).

Let us note that the PF jacket sections and the CS jacket sections call for similar mechanical tests at cryogenic temperatures [98,126-127], as well as similar PAUT and ECT inspections. The PF conductor production relies on the same jacketing facilities as the TF conductors, with dedicated welding stations and sturdier compaction machines.

5.4 Other Nb-Ti Conductors

Strand type 2 has also been qualified for use in CC and CB conductors [123] while an additional SULTAN sample is required to complete MB qualification. This sample is presently being assembled at CRPP and will be tested before the end of 2013.

CN has completed the production of the ~23 tons of Nb–Ti strand type 2 required for CC (see As shown in Figure 44(b)) and is proceeding with the production of the CC and CB conductors.

6. Conclusion

The ITER project offers many technical and management challenges but is an incredible human adventure and will become a milestone in the history of science. In spite of a difficult environment and tough constraints, but thanks to a good collaborative spirit and mutual trust and understanding at the technical level, the ITER conductor production is moving forward in all 6 ITER members involved (CN, EU, JA, KO, RF and US).

TF conductors are well into production, with ~95% of the required Nb_3Sn strands and more than half of the conductor unit lengths already completed. PF strand and conductor productions have been launched in RF/EU and CN; the first PF5 copper dummy conductor has been delivered from China to the ITER site in June 2013 and the first PF1 pre-dummy conductor has been delivered from EU to RF. CC and CB conductors are also in the production phase. A technical solution has been found for the challenging CS conductors and the production for the bottom module of the CS coil stack module (CS3L) has been launched.

As ITER conductor production is reaching its peak, the focus of the activities will naturally shift to coil manufacture. Let us hope that the ITER partners involved in this work will be animated by the same desire to transcend their domestic constraints and cultural habits so as to pursue the noble goal of bringing together the peoples of the world to build the ITER machine and, beyond, develop a safe, clean and sustainable energy source.

Acknowledgement

The authors wish to warmly thank their collaborators around the world who make this work possible, including: L. Delong, E. Niu, H. Li, S. Liu and M. Wang (CN-DA), C. Li, J. Qin and Y. Wu (ASIPP), T. Boutboul, P. Readman and E. Viladiu (F4E), A. della Corte, A. di Zenobio, L. Muzzi and S. Turtu (ICAS), K. Hamada (now at ITER IO), T. Isono, Y. Nabara, Y. Nunoya, K. Okuno, H. Ozeki and Y. Takahashi (JAEA), K. Jung, K. Kim, S.P. Kwon and S.H. Park (NFRI), A. Krasilnikov, D. Kravtsov, S. Lelekhov, V. Pantsyrny and V. Tronza (RF-DA), L. Potanina and V. Vysotsky (VNIIKP), K. Chan, N. Martovetsky and W. Reiersen (US-IPO), T. Painter (HPM) and J. Parrel (OST). The authors are indebted to S. Sgobba (CERN) for his reactivity, dedication and in depth knowledge of the properties, manufacturing processes and inspection techniques of steel products and to P. Bruzzone, B. Stepanov and the technical crew at CRPP for SULTAN sample preparation and tests. The authors also wish to thank the design reconciliation dream team: D. Ciazynski and A. Torre (CEA), H. Bajas (CERN), C. Calzolaio (CRPP), V. Aubin and D. Durville (ECP), D. Larbalestier, P. Lee and C. Sanabria (Florida State University), A. Nijhuis, G. Rolando and C. Zhou (Twente University), M. Breschi (University of Bologna) and M. Jewell (University of Wisconsin at Eau Claire) for their continuous and innovative contributions. Special thanks to D. Leroy (formerly from CERN), who was instrumental in developing and reviewing technical requirements, and to A. Ghosh (BNL), B. Turck (formerly from CEA), B. Strauss (US-DOE) and A. Yamamoto (KEK), eminent members of the External Conductor Procurement Review Committee, who helped drafting procurement arrangements and defining QA/QC requirements. Finally, this work would not have been possible without the active management support of G. Johnson (2007-2010) and R. Haange (2011-2013) and the mothering of C. Foucher de Brandois, C. Gregory and M. O'loughlin.

Disclaimer

The views and opinions expressed herein do not necessarily reflect those of the ITER Organization

References

[1] Ikeda K 2010 ITER on the road to fusion energy *Nucl. Fusion* 50 014002
[2] Clery D 2013 A Piece of the sun: the quest for fusion energy *Overlook Press*
[3] Holtkamp N 2009 The status of the ITER design *Fusion Engineering and Design* 84 98-105
[4] Mitchell N *et al* 2008 The ITER magnet system *IEEE Trans. Appl. Supercond.* 18 435–40
[5] Bonito Oliva A *et al* 2014 Progress in the F4E procurement of the EU ITER TF coils *presented to MT23 and submitted for publication to IEEE Trans. Appl. Supercond.*
[6] Koizumi N *et al* 2012 Development of ITER TF coil in Japan *IEEE Trans. Appl. Supercond.* 22 4200404
[7] Libeyre P *et al* 2014 Moving towards manufacture of the ITER central solenoid *presented at MT23 and submitted for publication to IEEE Trans. Appl. Supercond.*
[8] Lim B S *et al* 2012 Development of the ITER PF coils *IEEE Trans. Appl. Supercond.* 22 4201404
[9] Wei J *et al* 2014 Progress of the ITER correction coils in China *presented to MT23 and submitted for publication to IEEE Trans. Appl. Supercond.*
[10] Lu K *et al* 2014 Progress of the ITER feeder in China *presented at MT23 and submitted for publication to IEEE Trans. Appl. Supercond.*
[11] Ballarino A *et al* 2012 Design of the HTS current leads for ITER *IEEE Trans. Appl. Supercond.* 22 4800304
[12] Denz R *et al* 2014 Upgrade of the protection system for the superconducting elements of the LHC During LS1 *IEEE Trans. Appl. Supercond.* 24 4000604
[13] Coetana M *et al* 2010 Quench detection in the ITER magnet system LS1 *IEEE Trans. Appl. Supercond.* 20 427-430
[14] Hoenig M O and Montgomery D B 1975 Dense supercritical-helium cooled superconductors for large high field stabilized magnets *IEEE Trans. Magn. MAG-11* 569–572
[15] Devred A *et al* 2012 Status of ITER conductor development and production *IEEE Trans. Appl. Supercond.* 22 4804909
[16] Wu Y et al 2013 Manufacturing of the ITER conductors in China *IEEE Trans. Applied Superconductivity* 23 4802004
[17] Liu S *et al* 2014 Progress on TF and PF conductor for ITER in China *presented at MT23 and submitted to IEEE Trans. Applied Superconductivity*
[18] Boutboul T *et al* 2014 Status of the procurement of the European superconductors for the ITER magnets *presented at MT23 and submitted to IEEE Trans. Applied Superconductivity*
[19] Takahashi Y *et al* 2011 Technology development and mass production of Nb_3Sn conductors for ITER toroidal field coils in Japan *Nucl. Fusion* 51 113015 (11pp)
[20] Park SH *et al* 2014 Overview of conductor production for ITER Toroidal Field Magnet in Korea *presented at MT23 and submitted to IEEE Trans. Applied Superconductivity*
[21] Vysotsky V S *et al.* 2012 Status and achievements in production of ITER TF conductors and PF cables in Russian Cable Institute production *IEEE Trans. Appl. Supercond.* 22 4200505
[22] Devred A *et al* 2013 Conductor qualification program for the ITER Central Solenoid *IEEE Trans. Appl. Supercond*. 23 6001208
[23] Li H *et al* 2014 Qualification on the ITER Correction Coils and its conductor *presented at MT23 and submitted to IEEE Trans. Applied Superconductivity*
[24] Qin J *et al* 2013 Manufacture of ITER feeder sample conductors *Fusion Engineering and Design* 88 1461– 1464
[25] Pantsyrny V *et al* 2008 Nb_3Sn material development in Russia *Cryogenics* 48 354–370

[26] Park P and Kim K 2008 Status of Nb_3Sn strand development in Korea *Cryogenics* 48 347–353
[27] Li C G 2010 Investigation of superconducting properties of Nb_3Sn strands by Internal Tin process for ITER 20 1484-1487
[28] Liu W T *et al* 2010 Development of fine filament NbTi superconducting strands for ITER *IEEE Trans. Applied Superconductivity* 20 1504-1506
[29] Jewell M C *et al* 2010 World-wide benchmarking of ITER Nb_3Sn strand test facilities *IEEE Trans. Appl. Supercond.* 20 1500–1503
[30] Kikuchi K *et al* 1997 Development and manufacturing of bronze-processed Ta-added Nb_3Sn wires for the ITER *J. Cryog. Soc. Japan* 32 167–72 (in Japanese)
[31] Miyazaki T *et al* 2004 Development of Nb_3Sn superconducting wires for high-field magnets *J. Cryog. Soc. Japan* 39 415–21 (in Japanese)
[32] Nabara Y *et al* 2010 Procurement of Nb_3Sn superconducting conductors in *ITER J. Plasma Fusion Res. SERIES 9* 270-275
[33] Kanithi H *et al* 2012 Results of ITER-TF stand production at Luvata 2012 *Proceedings of ICEC 24-ICMC 2012* edited by K. Funaki, A. Nishimura, Y. Kamioka, T. Haruyama and H. Kumakura 791-794
[34] Parrell J A *et al* 2009 Internal tin Nb_3Sn conductors engineered for fusion and particle accelerator applications *IEEE Trans. Applied Superconductivity* 19 2573-2579
[35] Field M B *et al* 2014 Optimizing Nb_3Sn conductors for high field applications *presented at MT23 and submitted to IEEE Trans. Applied Superconductivity*
[36] Sytnikov V *et al* 1997 Development and manufacturing of superconducting Cable-In-Conduit Conductors for ITER *IEEE Trans. Applied Superconductivity* 7 1364-1367
[37] Hamada K *et al* 2011 First qualification of ITER Toroidal Field Coil conductor jacketing *Fusion Engineering and Design* 86 1506–1510
[38] della Corte A *et al* 2013 ITER and JT-60SA conductor production at ICAS *IEEE Trans. Applied Superconductivity* 23 4200904
[39] della Corte A *et al* 2013 ITER and JT-60SA conductor production at ICAS *IEEE Trans. Appl. Supercond.* 23 4200904.
[40] Seo K *et al* 2010 Implementation of the ITER conductor database *IEEE Trans. Applied Superconductivity* 20 499–502
[41] Bruzzone P *et al* 2002 Upgrade of operating range for SULTAN test facility *IEEE Trans. Appl. Supercond.* 12 520–523
[42] Painter T 2012 *private communication*
[43] Takahashi Y *et al* 2013 Cable twist pitch variation in Nb_3Sn conductors for ITER Toroidal Field coils in Japan *IEEE Trans. Appl. Supercond.* 23 4801504
[44] Bruzzone P *et al* 2010 Results of Thermal Strain and Conductor Elongation upon Heat Treatment for Nb_3Sn Cable-in-Conduit Conductors *IEEE Trans. Appl. Supercond.* 20 470-473
[45] Mitchell N 2005 Finite element simulations of elasto-plastic processes in Nb_3Sn strands *Cryogenics* 45 501–515
[46] van Lanen E P A and Nijhuis A 2009 JackPot: A novel model to study the influence of current non-uniformity and cabling patterns in cable-in-conduit conductors *Cryogenics* 50 139–148
[47] Breschi M *et al* 2012 Results of the TF conductor performance qualification samples for the ITER project *Supercond. Sci. Technol.* 25 095004 (17pp)
[48] Marsh S A *et al* 2013 Results of the TFEU6 sample tested in SULTAN Conductors *IEEE Trans. Appl. Supercond.* 23 4200204
[49] Bellina F *et al* 2010 Analysis of the ITER Nb_3Sn SULTAN sample test conditions with different joint technologies *IEEE Trans. Applied Superconductivity* 20 482-486

[50] van Lanen E P A and Nijhuis A 2011 Numerical analysis of the DC performance of ITER TF samples with different cabling pattern based on resistance measurements on terminations *Supercond. Sci. Technol.* 24 085010
[51] Breschi M *et al* 2009 Electromagnetic analysis of the voltage-temperature characteristics of the ITER TF conductor samples *IEEE Trans. Applied Superconductivity* 19 1512-1515
[52] Ciazynski D 2007 Review of Nb_3Sn conductors for ITER *Fusion Engineering and Design* 82 488–497
[53] Bruzzone P *et al* 2012 Test results of ITER conductors in the SULTAN Facility *Proceedings of 24th IAEA Fusion Energy Conference – IAEA CN-197* 536
[54] Stepanov B *et al* 2013 SULTAN test facility: Summary of recent results *Fusion Engineering and Design* 88 282–285
[55] Oh D K *et al* 2010 Performance Test of TFKO2 Qualification Sample of ITER TF *Conductor IEEE Trans. Applied Superconductivity* 20 458-461
[56] Kwon S P *et al* Preliminary performance test results of first CICC from Korea destined for an ITER TF magnet *IEEE Trans. Applied Superconductivity* 22 *IEEE Trans. Applied Superconductivity* 23 4201705
[57] Tronza V I *et al* 2013 Testing of RF 100 m TF qualification conductor in the SULTAN test facility *IEEE Trans. Applied Superconductivity* 23 9500805
[58] Tronza V I *et al* 2014 Test results of RF ITER TF conductors in the SULTAN test facility *presented at MT23 and submitted to IEEE Trans. Applied Superconductivity*
[59] Nunoya Y *et al* 2011 Test result of a full-size conductor developed for the ITER TF coils *IEEE Trans. Appl. Supercond.* 21 1982–1986
[60] Nabara Y *et al* 2012 Examination of mass-produced Nb_3Sn conductors for ITER Toroidal Field coils in Japan *IEEE Trans. Applied Superconductivity* 22 4804804
[61] P. Bruzzone *et al* 1996 Benchmark testing of Nb_3Sn strands for the ITER Model Coil, *Adv Cryog Eng (Mat)* 42B 1351
[62] Nijhuis A *et al* 2013 The effect of axial and transverse loading on the transport properties of ITER Nb_3Sn strands *Supercond. Sci. Technol.* 26 084004 (19pp)
[63] A. Devred *et al* 2012 Strain redistribution effects on current-sharing measurements on straight samples of large Nb_3Sn cable in conduit conductors *Supercond. Sci. Technol.* 25 054009
[64] Kajitani *et al* 2013 Analytical study of degradation of CIC conductor performance due to strand bending and buckling *IEEE Trans. Applied Superconductivity* 23 6001505
[65] Tsuji *et al* 2001 ITER R&D: Magnets: Central Solenoid Model Coil *Fusion Engineering and Design* 55 153–170
[66] Khodak A *et al* 2013 Optimization of ITER Central Solenoid Insert design *Fusion Engineering and Design* 88 1523-1527
[67] N. Martovetsky *et al* 2002 Test of the ITER Central Solenoid Model Coil and CS Insert *IEEE Trans Applied Superconductivity* 12 600–605
[68] N. Mitchell 2007 Assessment of conductor degradation in the ITER CS insert coil and implications for the ITER conductors *Supercond. Sci. Technol.* 20 25–34
[69] Miyatake T *et al* 2012 Influence of wire parameters on critical current versus strain characteristics of bronze processed Nb_3Sn superconducting wires *IEEE Trans. Applied Superconductivity* 22 4805005
[70] Hemmi T *et al* 2012 Test results and investigation of T_{cs} degradation in Japanese ITER CS conductor samples *IEEE Trans. Applied Superconductivity* 22 4803305
[71] Bruzzone P *et al* 1996 Conductor fabrication for the ITER Model Coils *IEEE Trans. Magn.* 32 2300-2303

[72] Mitchell N *et al* 1998 Conductor development for the ITER magnets *Proc. of the 15th Int. Conf. on Magnet Technology L. Liangzhen, S. Guoliao, Y. Luguang, eds. Beijing: Science Press* 347-352
[73] Bessette D *et al* 1993 Fabrication and test results of the 40 kA CEA conductor for NET/ITER *Proc. of the 17th Symposium on Fusion Technology C. Ferro, M. Gasparotto, H. Knoepfel, eds. Amsterdam: North Holland*
[74] Bessette D 2014 Design of a Nb_3Sn cable-in-conduit conductor to withstand the 60,000 electromagnetic cycles of the ITER Central Solenoid *presented at MT23 and submitted for publication to IEEE Trans. Applied Superconductivity*
[75] Nijhuis A *et al* 2012 Optimisation of ITER Nb_3Sn CICCs for coupling loss, transverse electromagnetic load and axial thermal contraction *Supercond. Sci. Technol.* 25 015007
[76] Nabara Y *et al* 2014 Impact of cable twist pitch on T_{CS} degradation and AC loss in Nb_3Sn conductors for ITER Central Solenoid tests *IEEE Trans. Applied Superconductivity* 24 4200705
[77] Calzolaio C *et al* 2012 In situ measurements of Cable in Conduit Conductors via an inductive method *IEEE Trans. Applied Superconductivity* 22 9002604
[78] Calzolaio C *et al* 2013 Monitoring of the thermal strain distribution in CICCs during the cyclic loading tests in SULTAN method *IEEE Trans. Applied Superconductivity* 23 4200404
[79] Hemmi T *et al* 2013 Neutron diffraction measurement of internal strain in the first Japanese ITER CS conductor sample *Supercond. Sci. Technol.* 26 084002 (6pp)
[80] Calzolaio C and P. Bruzzone 2014 Analysis of the CICCs performance through the measurement of the thermal strain distribution of the Nb_3Sn filaments in the cable cross section *presented at MT23 and submitted for publication to IEEE Trans. Applied Superconductivity*
[81] Bajas H *et al* 2010 Numerical simulation of the mechanical behaviour of ITER cable-in-conduit conductors *IEEE Trans. Appl. Supercond.* 20 1467–70
[82] Bajas H *et al* 2012 A. Approach to heterogeneous strain distribution in cable-in-conduit conductors through finite element simulation *IEEE Trans. Appl. Supercond.* 22 4803104
[83] Bajas H *et al* 2012 Finite element modeling of cable in conduit conductors *Supercond. Sci. Technol.* 25 054019
[84] Jewell M *et al* 2003 The influence of Nb3Sn strand geometry on filament breakage under bend strain as revealed by metallography *Supercond. Sci. Technol.* 16 1005–11
[85] Sheth M K *et al* 2011 Procedures for evaluating filament cracking during fatigue testing of Nb_3Sn strands *Advances in Cryogenic Engineering* 58 201-208
[86] Sanabria C *et al* 2012 Evidence that filament fracture occurs in an ITER toroidal field conductor after cyclic Lorentz force loading in SULTAN *Supercond. Sci. Technol.* 25 075007 (11pp)
[87] Mitchell N *et al* 2013 Electro-mechanical effects in Nb_3Sn Cable in Conduit Conductors: use of imperfect superconductors in cable in conduit conductors *presented at MEM13 and accepted for publication in Supercond. Sci. Technol.*
[88] Takahashi Y *et al* 2014 Cabling technology of Nb_3Sn conductor for ITER Central Solenoid *presented at MT23 and submitted for publication to IEEE Trans. Applied Superconductivity*
[89] Farinon S *et al* 2008 Nb_3Sn wire layout optimization to reduce cabling degradation *IEEE Trans. Appl. Supercond.* 18 984-988
[90] Bottura L and A Devred 2013 Cable design optimization for LTS applications *private communication*

[91] Sumption M D and Collings E W 1995 Chromium diffusion into plated Nb,Sn strands deduced from electrical resistivity measurement *IEEE Trans. Applied Superconductivity* 5 1925-1928
[92] Fetisov S S *et al* 2014 Residual Resistance Ratio in Nb_3Sn strands during ITER TF conductor manufacture and after SULTAN tests *presented at MT23 and submitted for publication to IEEE Trans. Applied Superconductivity*
[93] Horsthemke H 2008 Chromium deposition by trivalent and hexavalent processes for functional and decorative applications *private communication*
[94] Pong I *et al* 2012 Worldwide benchmarking of ITER internal tin Nb_3Sn and Nb-Ti atrands test facilities *IEEE Trans Appl. Supercond.* 22 4802606
[95] Bottura L and Bordini B 2009 $J_C(B,T,\varepsilon)$ parameterization for the ITER Nb_3Sn production *IEEE Trans Appl. Supercond.* 19 1521-1524
[96] Bordini B *et al* 2011 Magnetization and inter-filament contact in HEP and ITER bronze-route Nb_3Sn wires *IEEE Trans Appl. Supercond.* 21 3373-3376
[97] DeLong W T 1960 A modified phase diagram for stainless steel weld metals *Met. Prog.*, 77 98
[98] Vostner A *et al* 2013 Benchmarking of mechanical test facilities related to ITER CICC steel jackets *IEEE Trans. Appl. Supercond.* 23 9500705
[99] Weiss KP *et al* 2010 Tensile test results on compacted and annealed 316LN material *Advances in Cryogenic Engineering AIP Conference Proceedings* 1219 3-8
[100] Hamada K *et al* 2008 Development of jacketing technologies for ITER CS and TF conductor *Advances in Cryogenic Engineering Materials* 54 76-83
[101] Hamada K *et al* 20012 Effect of specimen shape on the elongation of 316LN jacket used in the ITER Toroidal Field coil *Advances in Cryogenic Engineering AIP Conference Proceedings* 1435 55-62
[102] Park S H *et al* 2012 The Effect of plastic deformation on low temperature mechanical and magnetic properties of Austenite 316LN tube for ITER TF conductor *IEEE Trans. Appl. Supercond.* 22 7800204
[103] Qin J *et al* 2012 Mechanical test on the ITER TF jacket *Cryogenics* 52 336–339
[104] Anashkin O P *et al* 2012 Tensile tests of ITER TF conductors jacket materials *AIP Conference Proceedings* 1435 117
[105] Spigo G 2013 Assessment of ASG unspooling device for TF coil winding *private communication*
[106] Nakajima H *et al* 2004 Development of low Carbon and Boron added 22Mn -13Cr – 9Ni – 1Mo – 0.24N steel (JK2LB) for jacket which undergoes Nb_3Sn heat treatment *IEEE Trans. Applied Supercond.* 14 1145-1148
[107] Hamada K *et al* 2007 Optimization of JK2LB chemical composition for ITER Central Solenoid conduit material *Cryogenics* 47 174–182
[108] Arnaud J P and Eveilleau M 2011 M Nitronic 50 Base Material Heat # A11371 Thermal Expansion *CERN NOTE SBT/CT/11-68*
[109] Libeyre P *et al* 2012 Addressing the technical challenges for the construction of the ITER Central Solenoid *IEEE Trans. Applied Supercond.* 22 4201104
[110] Libeyre P *et al* 2011 Conductor jacket development to meet the mechanical requirements of the ITER central solenoid coils *Fusion Engineering and Design* 86 1553-1557
[111] Sgobba S *et al* 2012 Progress in production and qualification of stainless steel jacket material for the conductor of the ITER Central Solenoid *IEEE Trans Appl. Supercond.* 22 7800104
[112] Nylas A *et al* 2012 Fatigue crack growth rate and fracture toughness of ITER central solenoid jacket materials at 7 K *AIP Conference Proceedings* 1435 47

[113] Hamada K *et al* 2012 Preparation for the ITER Central Solenoid conductor manufacturing *IEEE Trans Appl. Supercond.* 22 4203404
[114] Sgobba S *et al* 2013 A comparative assessment of metallurgical and mechanical properties of two austenitic stainless steels for the conductor jacket of the ITER Central Solenoid *Fusion Engineering and Design* 88 2484-2487
[115] Tsuchiya Y *et al* 1998 Residual stress for a jacket material for ITER superconducting coils *Physics B* 241-243 1264-1266
[116] Wong F M G *et al* 1996 Residual stresses in superconducting jackets after compaction *Proc. of 16th Int. Cryo. Eng. Conf. and Int. Cryo. Mat. Conf.*
[117} Walker K 1970 The effect of stress ratio during crack propagation and fatigue for 2024-T3 7005-T6 Aluminum ASTM STP 462 1-14
[118] Jong C Freudenberg K Myatt L and Cochran K 2013 Maximum allowable defect size for CS conduit unit length (7m) and butt-welds *private communication*
[119] Ozeki H *et al* 2014 Establishment of production process of JK2LB jacket section for ITER CS tests *presented at MT23 and submitted for publication to IEEE Trans. Applied Superconductivity*
[120] Bauser M Sauer G Siegert K (eds) 2006 Extrusion, Second Edition *ASM International, Materials Park, Ohio 44073-0002*
[121] Sgobba S 2013 *personal communication*
[122] Stepanov B *et al* 2012 Test Results of Three Poloidal Field Superconducting Samples in SULTAN *IEEE Trans Appl. Supercond.* 22 4803504
[123] Pong I *et al* 2012 Current sharing temperature of NbTi SULTAN samples compared to prediction using a single pinning mechanism parameterization for NbTi strand *Supercond. Sci. Technol.* 25 054011 (9pp)
[124] Reccia L *et al* 2011 Preparation of PF1/6 and PF2 Conductor Performance Qualification Sample *IEEE Trans Appl. Supercond*. 21 1930 - 1933
[125] Bruzzone P *et al* 2005 Test results of the ITER PF insert conductor short sample in SULTAN *IEEE Trans Appl. Supercond.* 15 1351 - 1354
[126] Liu H J *et al* 2011 Mechanical tests on the ITER PF 316L jacket after compaction Cryogenics 51 (2011) 234–236
[127] Qin J *et al* 2012 Fatigue tests on the ITER PF jacket *Cryogenics* 52 486–490